

POLITECNICO DI TORINO

Master's Degree in Energy and Nuclear Engineering



Master's Degree Thesis

Characterization and modeling of alkaline electrolyzers for hydrogen production

Supervisors

Prof. Mika JÄRVINEN

Prof. Massimo SANTARELLI

Candidate

Andrea PANCOTTO

Academic Year 2020-2021

Graduation Session December 2021

Abstract

This master thesis proposes a model of an alkaline electrolysis plant. The aim is to determine the performance of a complete hydrogen production system at different working conditions. An explanation and characterization of the fundamental aspects of water electrolysis is carried out and a modeling approach is proposed for the interpretation of the system. Semi-empirical equations are used for describing the polarization behaviour, the Faraday efficiency and the gas purity variation with the current. The required parameters are calculated with a retrofitting procedure on Matlab, on the basis of experimental data. The electrolyzer stack block is defined in Aspen Custom Modeler and exported to Aspen Plus, where it is implemented in the complete plant. An original approach is used considering the process of salt dissociation in ions. A parametric study is conducted showing that the system efficiency could benefit from an increase of stack temperature and decrease of operational pressure. The hydrogen flow rate demonstrated to be sensible to both the thermodynamic quantities. The temperature showed to increase the electricity conversion into useful energy for the process, reducing the production of excessive heat. Further improvements could be carried out in the future accounting for drying and purification unit for the hydrogen.

Keywords: hydrogen, alkaline electrolysis, mathematical modeling, Aspen Plus, Aspen Custom Modeler, Matlab

Acknowledgements

Kiitos Suomi.

I am grateful to Professor Mika Järvinen for the opportunity to work on my final project at Aalto University, to PhD candidate Shouzhuang Li for his advises during the entire project, to Mohamed Magdeldin for the expertise devoted to help me out of obstacles, to all those people that have warmly welcomed me to Helsinki.

Un grazie anche al Professore Massimo Santarelli che mi ha permesso di trattare un argomento di grande interesse. Grazie a tutti quelli che mi sono stati vicino in questo percorso e non solo. Grazie a coloro che poi la vita ci ha fatto prendere percorsi differenti.

Il ringraziamento più grande va a mia madre e mio padre, coloro che mi hanno sempre sostenuto, coloro che hanno sempre creduto in me, coloro che mi hanno insegnato la forza della determinazione; è soprattutto a loro se sono riuscito a coronare questo traguardo.

“Ad astra”
Andrea Pancotto
3 Dicembre 2021

Table of Contents

| | |
|--|------|
| List of Tables | VII |
| List of Figures | VIII |
| Acronyms | XI |
| 1 Introduction | 1 |
| 1.1 Objectives of the work | 4 |
| 1.2 Methods | 4 |
| 1.3 Outline of the thesis | 5 |
| 2 Fundamentals of water electrolysis | 6 |
| 2.1 Working principle | 6 |
| 2.1.1 Hydrogen evolution reaction | 8 |
| 2.1.2 Oxygen evolution reaction | 9 |
| 2.1.3 Faraday law | 9 |
| 2.2 Thermodynamics | 9 |
| 2.2.1 Thermal behaviour of the cell and mode of operation | 13 |
| 2.2.2 Thermodynamic losses | 15 |
| 2.3 Electrochemistry | 15 |
| 2.3.1 Polarization curve | 16 |
| 2.3.2 Transport phenomena | 17 |
| 2.3.3 Electrical circuit analogy | 21 |
| 2.3.4 Efficiency evaluation | 22 |
| 2.3.5 Specific energy consumption | 25 |
| 2.3.6 Specific water consumption | 26 |
| 2.4 Advanced alkaline solution | 27 |
| 2.4.1 The problem of bubbles | 27 |
| 2.4.2 Ways to enhance water electrolysis | 28 |
| 2.4.3 Safety issues | 28 |
| 2.5 Materials employed in alkaline electrolyzer and design | 29 |

| | | |
|----------|--|-----------|
| 2.5.1 | Electrode materials | 29 |
| 2.5.2 | Electrolyte materials | 30 |
| 2.5.3 | Diaphragm materials | 30 |
| 2.5.4 | Balance of the plant | 30 |
| 2.5.5 | Electrolyzer design | 30 |
| 2.6 | Future efforts | 32 |
| 3 | Mathematical modeling | 33 |
| 3.1 | Electrochemical model | 35 |
| 3.1.1 | Polarization behaviour | 35 |
| 3.1.2 | Faraday efficiency | 37 |
| 3.1.3 | Mass balance | 38 |
| 3.1.4 | Energy balance | 39 |
| 3.1.5 | System efficiency | 39 |
| 3.2 | Thermal model | 40 |
| 3.2.1 | Lumped thermal capacitance method | 40 |
| 3.3 | Gas purity model | 42 |
| 3.4 | Parameters fitting | 42 |
| 3.5 | Aspen modeling | 45 |
| 3.5.1 | Electrolytic stack model | 45 |
| 3.5.2 | System model | 46 |
| 4 | Results and Discussion | 48 |
| 4.1 | Coefficient estimation | 48 |
| 4.2 | Matlab simulations | 49 |
| 4.3 | Aspen Plus simulation | 51 |
| 4.3.1 | Study on explosive limits | 53 |
| 4.4 | Validation of Matlab model | 53 |
| 4.5 | Comparison with commercial systems | 57 |
| 4.6 | Parametric study | 58 |
| 5 | Conclusion | 62 |
| 5.1 | Future developments | 63 |
| A | Consideration of similar technologies | 64 |
| A.1 | Comparison with different electrolysis solutions | 64 |
| A.2 | Comparison within different alkaline electrolyzers | 65 |
| | Bibliography | 68 |

List of Tables

| | | |
|-----|---|----|
| 1.1 | Annual global hydrogen production share by source [4]. | 2 |
| 3.1 | Comparison table for different models. Starting from left: Ulleberg [11], Sánchez [64, 65], model proposed in this thesis. | 35 |
| 4.1 | Coefficient evaluation from experimental data. | 49 |
| 4.2 | Material flow composition at base case ($T=75^{\circ}\text{C}$ and $p=7$ bar). . . | 53 |
| 4.3 | Comparison table of the main electrolyzer model characteristic, with commercial datasheet by Cummins [76] and Nel hydrogen [77]. The data from the model are evaluated at 80°C and 7 bar. | 57 |
| A.1 | Comparison between different types of water electrolysis. Basic chemical reaction and operating temperature range [49]. | 66 |

List of Figures

| | | |
|-----|---|----|
| 1.1 | Benefits of hydrogen for the EU [2]. | 1 |
| 1.2 | Main methods for hydrogen production by energy sources. | 3 |
| 2.1 | Schematic representation of an alkaline electrolysis cell [12]. | 7 |
| 2.2 | Simplifying scheme of an electrolysis cell, representing: (a) inlet and outlet material, heat and power streams; (b) thermal behaviour. . . | 10 |
| 2.3 | Reversible and thermo-neutral voltage behaviour, function of temperature at $p = 1 \text{ bar}$ [20]. | 14 |
| 2.4 | Polarization curve. The contribution of different irreversible phenomena is highlighted in different colors. $V_{act,\Theta}$ is the contribution from bubble coverage of the electrodes, while $V_{act,e}$ is the contribution from the bubble-free electrodes [23]. | 16 |
| 2.5 | Complete electrical circuit analogy of resistances in the water electrolysis system [32]. | 22 |
| 2.6 | Unipolar (on the right) and bipolar (on the left) cell configuration [11]. | 31 |
| 3.1 | Procedure for the determination of the cell voltage parameters. The diamonds on the left express the experimental data evaluated at those conditions. | 44 |
| 3.2 | Aspen plus base-case model. The AEL block represents the alkaline electrolyzer stack modeled separately in ACM. | 47 |
| 4.1 | Fitted Polarization behaviour modeled (curve) and experimental data (dots). | 50 |
| 4.2 | Fitted Faraday efficiency (curve) and experimental data (dots). . . . | 50 |
| 4.3 | Fitted gas purity (curve) and experimental data (dots). | 51 |
| 4.4 | Aspen Plus base-case model solution. | 52 |
| 4.5 | Matlab vs Aspen plus comparison of operative cell voltage at different temperatures. | 54 |
| 4.6 | Matlab vs Aspen plus comparison of operative cell voltage at different pressures. | 54 |

| | | |
|------|---|----|
| 4.7 | Matlab vs Aspen plus comparison of Faraday efficiency at different temperatures. | 55 |
| 4.8 | Matlab vs Aspen plus comparison of Faraday efficiency at different pressures. | 55 |
| 4.9 | Matlab vs Aspen plus comparison of hydrogen in oxygen content at different temperatures. | 56 |
| 4.10 | Matlab vs Aspen plus comparison of hydrogen in oxygen content at different pressures. | 56 |
| 4.11 | Polarization behaviour (solid curves), electric power inlet (dotted curves) and excess heat production (dashed curves), evaluated at different temperatures ($p = 7 \text{ bar}$): (a) data from current model; (b) data from [54]. | 58 |
| 4.12 | Hydrogen flow rate (solid curves) and hydrogen crossover in the anode (dotted curves), evaluated at different temperatures ($p = 7 \text{ bar}$): (a) data from current model; (b) data from [54]. | 59 |
| 4.13 | Faraday efficiency (solid curves) and voltage efficiency (dotted curves), evaluated at different temperatures ($p = 7 \text{ bar}$): (a) data from current model; (b) data from [54]. | 59 |
| 4.14 | Polarization behaviour (solid curves), electric power inlet (dotted curves) and excess heat production (dashed curves), evaluated at different pressures ($T = 75^\circ\text{C}$): (a) data from current model; (b) data from [54]. | 60 |
| 4.15 | Hydrogen flow rate (solid curves) and hydrogen crossover in the anode (dotted curves), evaluated at different pressures ($T = 75^\circ\text{C}$): (a) data from current model; (b) data from [54]. | 60 |
| 4.16 | Specific energy consumption of the stack (solid curve) and global system efficiency (dotted curve), evaluated at $p = 7 \text{ bar}$: (a) data from current model; (b) data from [54]. | 61 |

Acronyms

ACM

Aspen Custom Modeler

AEL

Alkaline ELectrolyzer

BEV

Battery Electric Vehicle

CAPEX

CAPital EXpenditure

CCS

Carbon Capture and Storage

ENRTL

Electrolyte NonRandom Two Liquid

FCEV

Fuel Cell Electric Vehicle

GDL

Gas Diffusion Layer

HER

Hydrogen Evolution Reaction

HTO

Hydrogen-To-Oxygen

IRENA

International Renewable Energy Agency

LEL

Lower Explosion Limit

OCV

Open Circuit Voltage

OER

Oxygen Evolution Reaction

OTH

Oxygen-To-Hydrogen

P2P

Power To Power

PEM

Proton Exchange Membrane electrolyzer

PV

PhotoVoltaic

RES

Renewable Energy Sources

RDS

Rate Determining Step

SOEC

Solid Oxide Electrolysis Cell

STP

Standard Temperature and Pressure Conditions

TRL

Technology Readiness level

Chapter 1

Introduction

The EU Green Deal has the purpose of making Europe the first continent with a zero carbon impact. To reach this goal greenhouse gas emission reductions are required across every sector; renewable energy implementation and energy efficiency improvement can provide over 90% of the reduction in energy-related CO₂ emissions [1]. However, one third of energy-related emissions currently have no economically viable decarbonization options. Hydrogen is an energy carrier, it could be the link to allow renewable energy to reach the transport, building and industry sectors, for which electrification would be difficult otherwise. According to [2] hydrogen could provide up to 24% of total energy demand of Europe Union by 2050, in the more ambitious scenario (figure 1.1). In order to get the target of 2050, EU needs to reduce its CO₂ emission from 3500 Mt to 770 Mt. Almost 60% of the reduction could be represented by means of deploying available technologies, like solar and wind, while hydrogen could be responsible of helping reducing other 560 Mt of CO₂ emissions.

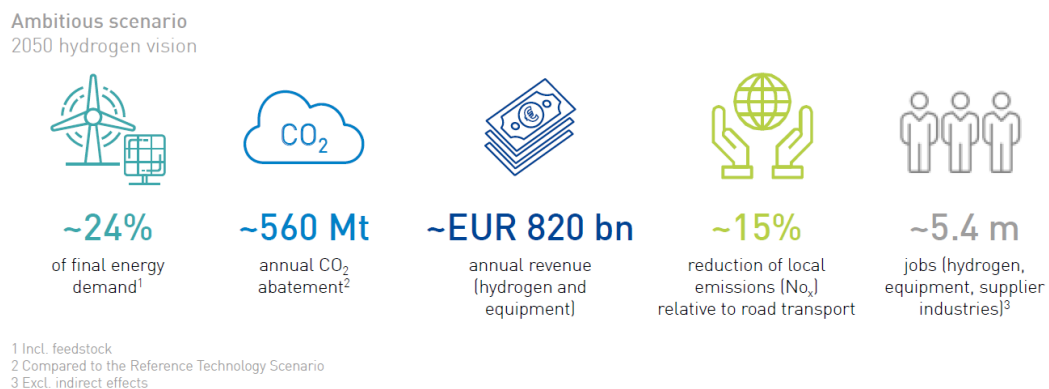


Figure 1.1: Benefits of hydrogen for the EU [2].

However significant challenges still need to be addressed in the hydrogen evolution chain. Since the climate change initiatives remains the most important driver for the use of clean hydrogen, the uncertainty of governments, pushing toward the transition to low-carbon energy, remain central. Most applications for low-carbon hydrogen are not cost-competitive without direct support of government [3]. Infrastructure is of particular importance when considering a new energy carrier such as hydrogen. Hydrogen pipelines and road delivery networks are fundamental and precondition for the spreading of FCEVs market. A last challenge concern the evolution of regulations and standards, which are currently limiting the hydrogen uptake [1]. They need to be updated, on an international agreed basis, in order to give hydrogen the possibility to fulfil its potential. That is why governments are playing a crucial role in the present and future of hydrogen.

The principal way to transform renewable energy into hydrogen is through water electrolysis. The readiest technology at a commercial stage are alkaline electrolyzers. However, around 96% of today hydrogen production is from fossil fuels [1, 4, 5], in particular the biggest share come from steam reforming of methane, as can be seen from the table below 1.1. Without carbon capture processes, the CO_2 , released from methane is released to the environment, becoming a problem for the environment [6].

Table 1.1: Annual global hydrogen production share by source [4].

| Source | Bm^3/yr | Share (%) |
|--------------|-----------|-----------|
| Natural gas | 240 | 48 |
| Oil | 150 | 30 |
| Coal | 90 | 18 |
| Electrolysis | 20 | 4 |
| Total | 500 | 100 |

There is the need to inverse the trend and make electrolysis, for production of green hydrogen, spread the market becoming more economically effective. That's why policy and financial support are of central importance in this early stage. Hydrogen contributes to sector coupling, playing a systemic role in the transition to RES increasing the flexibility across sectors, time and place [2]. It is a way to transport and distribute energy in medium and long term in addition to long distances.

Current technologies for the production of hydrogen are mainly water electrolysis and steam reforming, as said; less mature technologies comprehend biomass gasification and pyrolysis, thermochemical water splitting, photocatalysis, supercritical water gasification of biomass, and combined dark fermentation and anaerobic digestion [4]. The following figure 1.2 shows the different hydrogen production

technologies starting from primary energy sources (fossil and renewable) and the main end-uses. The main advantages of water electrolysis consist in no CO_2 emissions related to the conversion and to a higher purity hydrogen compared to other technologies; however, the cost of water electrolyzers is in general higher [7].

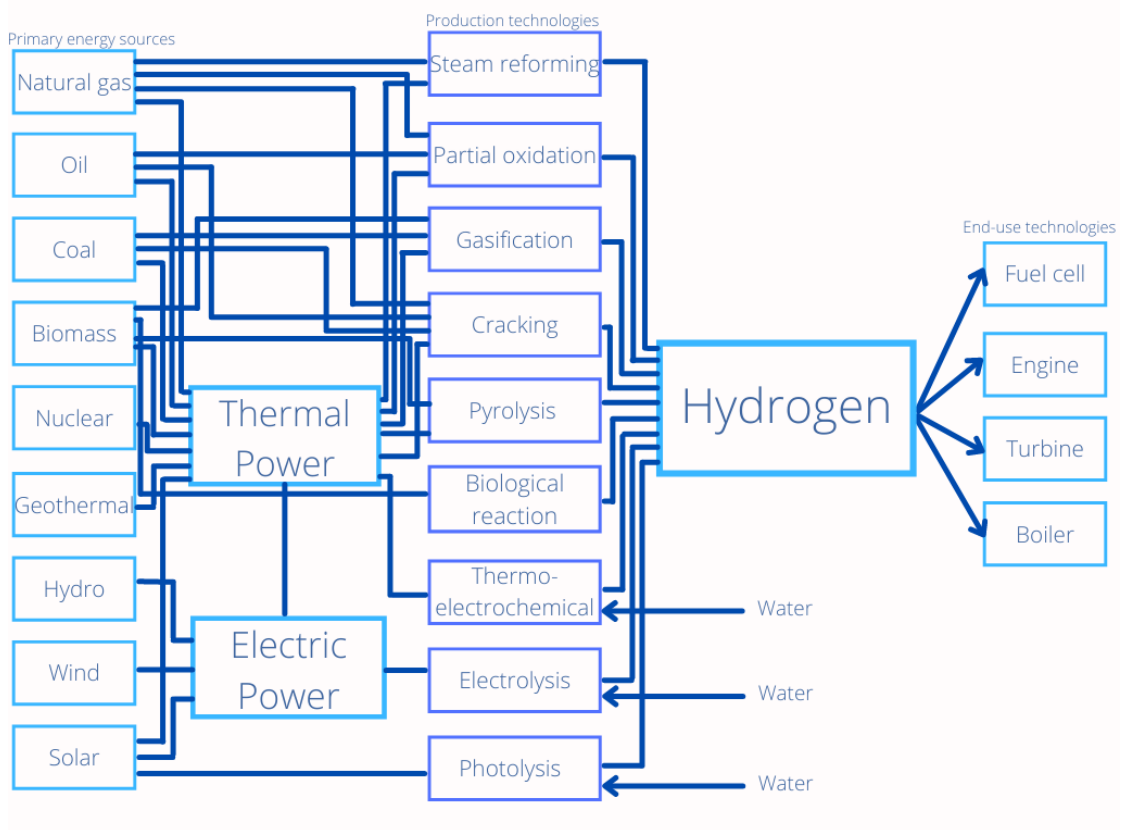


Figure 1.2: Main methods for hydrogen production by energy sources.

Water electrolysis presents 3 main technologies: alkaline electrolyzers (AEL), proton exchange membrane electrolyzers (PEM) and solid oxide electrolysis cells (SOEC). AEL represents the most mature technology from the moment that was employed in the chemical industry since 1920s [1]. It has a stack lifetime of around 80000 h, quite the double of PEM technology [1]. The installation costs in term of CAPEX are also lower if compared to PEM. On the other side PEM presents a smaller footprint and the capacity to work at higher pressure, making the pressurization costs more affordable, thinking as application in the automotive sector. PEM also allows more flexible operations having wider operation range and shorter response time. Regarding the application, both PEM and AEL are not suitable for the coupling in stand-alone plant due to the low load factor provided by renewable generation. SOEC is in early stage of development; the main problems

are related to the high temperature needed which make the efficiency to drop significantly, when the heat source is included in the calculation [7]. Nevertheless the problems, the SOEC have great expectations for the future due to its increased conversion efficiency, related to the high working temperatures, and the possibility of producing synthesis gas directly from steam and CO₂ [7].

It is concluded that, hydrogen is a viable energy carrier for the decarbonization of society. The ability of it to be produced from a wide variety of feedstocks and using a wide variety of processes makes it so that every region of the world could be able to produce much of their own energy. Hydrogen would be able to concentrate renewable energy also in those sectors where electrification is more difficult. The main enemies, at the present moment, are represented by costs. One way is, certainly, through regulations and policies. Another way is represented by a continuous research in technologies for the production of green hydrogen: electrolyzers. Alkaline electrolyzers are already at a commercial scale, however, more research is needed in order to have a continuous cost abatement, for making production of hydrogen from renewable energy feasible.

1.1 Objectives of the work

The objective of the thesis is to develop an Aspen Plus model for alkaline electrolyzers. It will be used for the evaluation of the technical performances of an hydrogen production system, in stationary operations. Especially, the model will be able to predict several operative parameters for the optimal characterization of a real plant. Different mathematical models are present in literature for the electrochemical description of electrolytic cells, but solely a poor literature consideration is showed on the developing of a complete hydrogen production facility on Aspen Plus. This work has the aim to close the gap between the mathematical modeling and software modeling, with the design of an electrolytic stack block.

1.2 Methods

As the first step, the model is created on Matlab to test it properly. The model is based on semi-empirical equations, which parameters are calculated by means of a non-linear retrofitting procedure on Matlab. All the relevant steps in the electrolysis process and mass and energy balances are included inside the electrolyzer block modeled in Aspen Custom Modeler. A complete hydrogen production system is implemented in Aspen Plus. It connects the alkaline electrolyzer stack to the separation unit and recirculation loop for the electrolyte. The performance of the system is measured and compared to find the best operational conditions. The created model could be used to investigate the operational parameters of a real

electrolysis plant and to examine performances in different stationary operations, in order to find the best operative conditions.

1.3 Outline of the thesis

After this short introduction on the role of hydrogen for the decarbonization of society and the importance of alkaline electrolysis for its production, the following chapter are presented:

Chapter 2 A detailed overview on the operating principles, thermodynamics and electrochemistry of the electrolysis phenomenon is explained. Architectures and material employed in the fabrication of commercial alkaline electrolyzers is presented.

Chapter 3 The description of the mathematical model of an alkaline electrolyzer is presented. The retrofitting procedure is performed in Matlab. The electrolyzer block is created in Aspen Custom Modeler and then exported into Aspen Plus, where a complete system for hydrogen production is characterized.

Chapter 4 Results are presented and discussed. A parametric study on the present system model is showed.

Chapter 5 Conclusions are presented for the main topics discussed in the thesis.

Chapter 2

Fundamentals of water electrolysis

Water electrolysis is the simplest way for producing green hydrogen. It permits to store the overproduction of electricity in a chemical form for long terms. With alkaline water electrolysis is intended the concept of using electricity for splitting the water molecule into oxygen and hydrogen using an alkaline solution as electrolyte. It is usually performed below 100°C at ambient pressure because of the liquid form of the electrolyte; but it can be operated also in pressure. Using a polymer membrane as electrolyte makes it possible to reach higher temperatures and a better dynamic behaviour (PEM). Higher temperatures could be reached using solid oxide as electrolyte, increasing the efficiency of the process (SOEC); however, these last concepts are not yet in the full industrial scale, TRL 8 and 6 respectively [8, 9].

The electrochemical cell is the fundamental component of an electrolyzer, it is composed of an electrode acting as anode and an electrode acting as cathode; they are connected by means of an external electric circuit and they are submerged in the electrolyte bath. A membrane act as a solid separator between the two electrochemical parts, avoiding the diffusion of O_2 and H_2 gas molecules. The potential of a single cell is limited, so different cells are connected in series forming stacks, and different stacks could be further connected together, to form the electrolyzer. The voltage imposed depends on the characteristics of the cell and the hydrogen production rate is proportional to the current density [10].

2.1 Working principle

The electrolysis cell is the fundamental device which makes it possible to transform deionized water into hydrogen and oxygen. This is possible following the reaction

2.1.



The water splitting reaction shows a variation of the Gibbs free energy positive ($\Delta G^\circ = +237 \text{ kJ/mol}$ at standard condition [11]), which means that the reaction is non-spontaneous and an external energy source must be applied to make it happen. The energy is applied in the form of electricity, as a potential through the electrodes submerged in the aqueous solution. A schematic design is illustrated in 2.1, where it is also possible to see the two half reactions at the anodic and cathodic side.

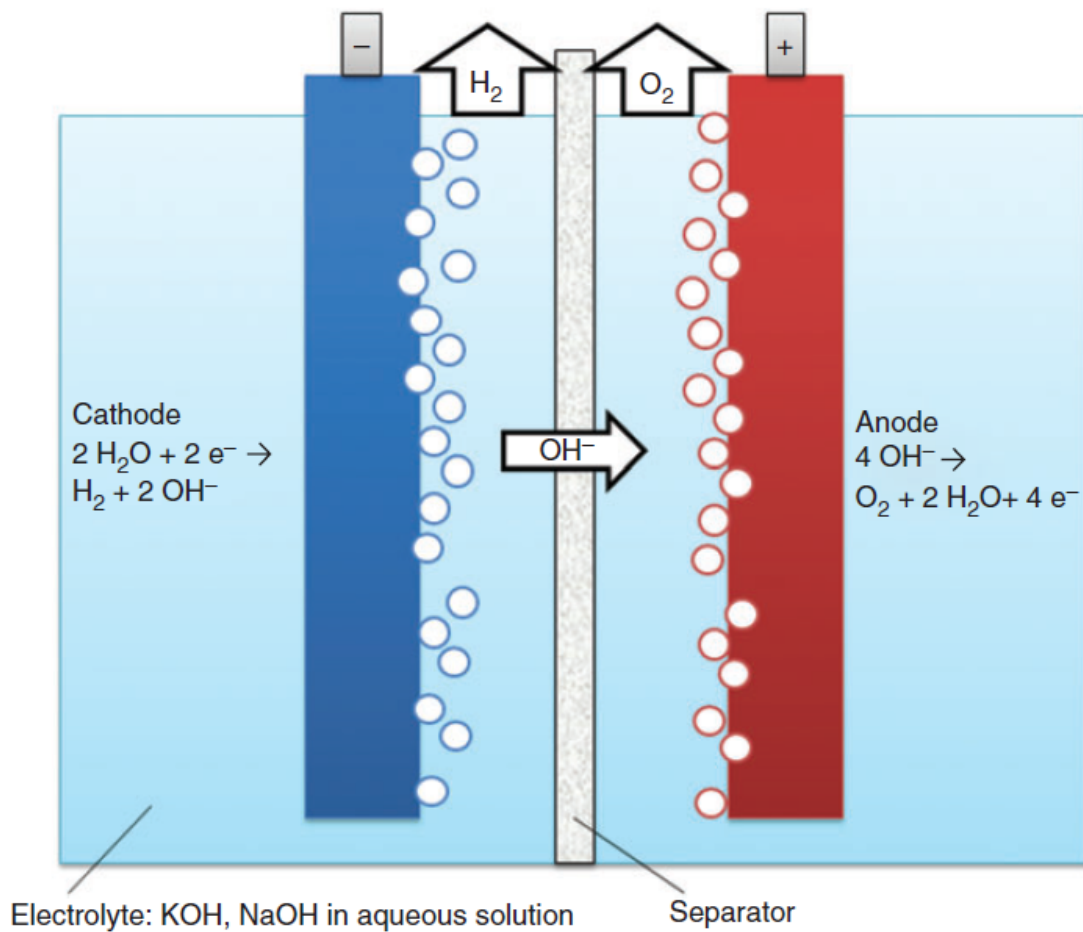
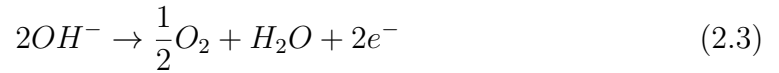
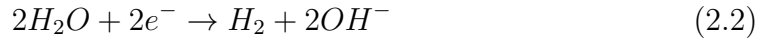


Figure 2.1: Schematic representation of an alkaline electrolysis cell [12].

The fundamental components are anode, cathode, electrolyte and separator. When an external DC source is applied, the electrons are consumed by water

molecule (H_2O) to form hydrogen. In order to balance the electrical charge, the hydroxide ions (OH^-) transfer through the separator, releasing the electron at the anode. The electrolyte is a solution consisting of water, and salt to improve the conductivity of ions. The concentration of salt, in the solution, increases the conductivity, which consequently increases the corrosion of the metal electrodes. The diaphragm act as a solid separator, in order to not mix the hydrogen and oxygen produced in the gas form.

The cathode and anode sub-reactions, respectively, can be defined as:

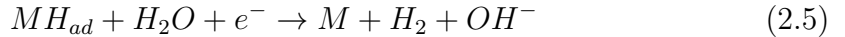


2.1.1 Hydrogen evolution reaction

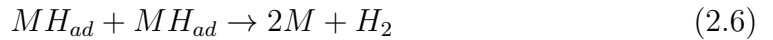
The hydrogen evolution reaction (HER) proceeds via the formula 2.2, with a standard electrode potential of $V^0 = -0.828 V$. It can be divided into two consecutive steps as illustrated [13]. First the water dissociation happen (Volmer step):



followed by the hydrogen emission (Heyrovsky step and Tafel step), respectively:



and

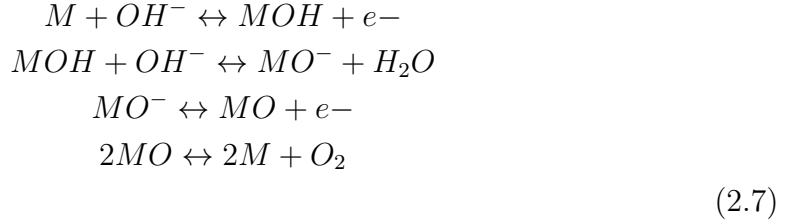


These two steps proceed in parallel, competing. The Heyrovsky step and Tafel step are lead by electrochemical and chemical desorption, respectively. Several intermediate steps are employed from the hydrogen adsorption or absorption to the emission of molecular hydrogen. The reaction rate depends on the morphology and the catalyst type, as the rate determining step (rds). The rds demonstrated to be the Tafel step when employing Ni-Fe-Pt catalysts [12].

The Volmer step is potential determining. This means that it determines the overpotential at which a specific current density could be reached. A potential determining step is different from a rate determining step, because in the first case they suffer from unfavorable thermodynamics but not necessarily from unfavorable kinetics [14].

2.1.2 Oxygen evolution reaction

The oxygen evolution reaction (OER) proceed via the reaction 2.3, with a potential of $V^0 = 0.401 V$. The mechanism steps of the OER in alkaline solution proposed by Kubisztal and Budniok [15], are:



The kinetics of the OER is slow and the RDS depends on the applied potential. Anode material, electrode surface and temperature are the major factor affecting the overpotential.

2.1.3 Faraday law

The Faraday law presents the relation between molecular species and charged species, and it is defined as follow:

$$I = \dot{n}_{i(R/P)} \cdot z_i \cdot F \tag{2.8}$$

where I is the current in $[A]$ both electronic and ionic; $\dot{n}_{i(R/P)}$ is the molar flow of a chemical species i for both reactant and product in $[mol/s]$; z_i is the charge number of chemical species i and represent the number of electrons involved in a oxidation or reduction reaction of the species i ; F is the Faraday constant ($F = 96487 C/mol$). In the case of water electrolysis 2 electrons are involved in semi-reactions, so $z_i = 2$, the equation 2.8 become:

$$I = \dot{n}_{i(R/P)} \cdot 2 \cdot 96487 \tag{2.9}$$

By means of equation 2.9 is evident the direct relationship between molar flow and current, by means of a constant factor.

2.2 Thermodynamics

The operations of an electrochemical cell could be described by means of fundamentals thermodynamics. An electrolyzer works converting electrical energy into chemical energy, in the form of hydrogen. Considering an electrochemical cell

operating at constant temperature and pressure, the energy requirements for the water electrolysis reaction is represented by the enthalpy of formation ΔH . It could be seen as the sum of two contributions: one electrical and the other in form of heat. The electrical contribution is defined as the change in Gibbs free energy ΔG . The thermal energy Q could be described as the product between the temperature at which the reaction occurs and the entropy change ΔS [16]. In mathematical form:

$$\Delta G = \Delta H - Q = \Delta H - T \cdot \Delta S \quad (2.10)$$

The sign of the Gibbs free energy determines the spontaneity of the reaction, while the enthalpy variation determines the thermal requirements. The process that occurs in a electrochemical cell is endothermic ($\Delta H > 0$) and non-spontaneous ($\Delta G > 0$).

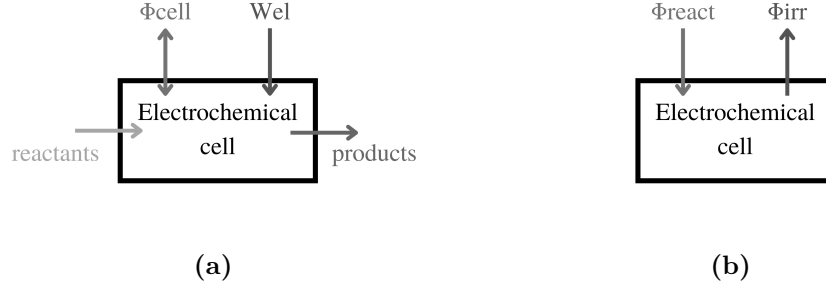


Figure 2.2: Simplifying scheme of an electrolysis cell, representing: (a) inlet and outlet material, heat and power streams; (b) thermal behaviour.

More in detail, applying the first and second laws of thermodynamics to the considered electrochemical cell in 2.2(a) with a $\Delta g_{react}^1 > 0$, in the case of electric work provided to the cell $W_{el} < 0$:

$$\Phi + W_{el} - \sum_P \dot{n}_P \cdot \bar{h}_P(T, p_i) + \sum_R \dot{n}_R \cdot \bar{h}_R(T, p_i) = 0 \quad (2.11)$$

$$\Phi/T - \sum_P \dot{n}_P \cdot \bar{s}_P(T, p_i) + \sum_R \dot{n}_R \cdot \bar{s}_R(T, p_i) = 0 \quad (2.12)$$

where Φ is the heat provided to the cell (negative when representing the excess heat); W_{el} is the electrical power provided to the cell (positive when entering the system); \bar{h}_P and \bar{h}_R are the molar entalpy of products and reactants respectively;

¹Lower case represents the molar values of Gibbs free energy, enthalpy and entropy.

T is the cell temperature (K); p_i is the partial pressure of species i ; \bar{s}_P and \bar{s}_R are the molar entropy of products and reactants respectively; the second law 2.12 is imposed to zero applying the condition of thermodynamic equilibrium. Normalizing by the number of moles of water:

$$\bar{q} + \bar{l} - \sum_P \nu_P \cdot \bar{h}_P(T, p_i) + \sum_R \nu_R \cdot \bar{h}_R(T, p_i) = 0 \quad (2.13)$$

$$\bar{q}/T - \sum_P \nu_P \cdot \bar{s}_P(T, p_i) + \sum_R \nu_R \cdot \bar{s}_R(T, p_i) = 0 \quad (2.14)$$

where \bar{q} is the molar quantity of heat [J/mol]; \bar{l} is the molar power; ν_P and ν_R are respectively the stoichiometric coefficients of products and reactants. Highlighting the entalpy variation of the reaction $\Delta\bar{h}_{react}$ and the entropy variation of the reaction $\Delta\bar{s}_{react}$:

$$\bar{q} + \bar{l} - \Delta\bar{h}_{react} = 0 \quad (2.15)$$

$$\bar{q}/T - \Delta\bar{s}_{react} = 0 \quad (2.16)$$

From the union of the two:

$$\bar{l} = \Delta\bar{h}_{react} - T\Delta\bar{s}_{react} = \Delta\bar{g}_{react} \quad (2.17)$$

This means that the electrochemical cell is not able to convert all the input work (electrical power) into chemical energy, but it is converted only into the Gibbs free energy $\Delta\bar{g}_{react}$ of the reaction.

Expressing the molar work \bar{l} in another way:

$$\bar{l} = W_{el}/\dot{n}_F \quad (2.18)$$

which became 2.19, applying 2.8:

$$\bar{l} = z_F F E \quad (2.19)$$

where E is the voltage difference [V] across the cell in equilibrium conditions; it is defined Nerst potential, equilibrium voltage or open circuit voltage (OCV).

Comparing equations 2.17 and 2.19 it is possible to obtain the Nerst equation:

$$OCV = \frac{\Delta\bar{g}_{react}(T, p_i)}{z_F F} \quad (2.20)$$

This fundamental relationship states that the voltage gradient OCV generated in condition of equilibrium, without transport phenomena, is dependent from the Gibbs free energy of the reaction $\Delta\bar{g}_{react}$. The equilibrium voltage is only function of the global reaction driven by the cell, it will depend from chemistry (reactants

and product) and from thermodynamic quantities (T, p). In standard condition (1 bar and $25^\circ C$), it corresponds to $1.23V$ (OCV^0).

Considering that molar Gibbs free energy could be expressed as:

$$\bar{g}(T, p_i) = \bar{g}(T, p_0) + RT \ln(p_i/p_0) \quad (2.21)$$

and applying it into 2.20

$$OCV = + \frac{\Delta \bar{g}_{react}(T, p_0)}{z_F F} + \frac{RT}{z_F F} \ln \frac{\prod^P (p_i/p_0)^{\nu_i}}{\prod^R (p_i/p_0)^{\nu_i}} \quad (2.22)$$

In order to obtain the product already in pressure the equilibrium potential E required will be higher, requiring higher W_{el} [17]. The term p_i/p_0 appears only imposing the hypothesis of ideal gas. The unique situation of equilibrium for the electrochemical cell is in case of open circuit.

Starting from the theoretical cell voltage (OCV) just described, it is possible to define other potentials related to the cell behaviour; the enthalpic voltage $V_{t,p}$ is defined as the ratio between the enthalpy of dissociation of liquid water into elements at a certain T and p over the electron transfer number times the Faraday constant [18]. In mathematical terms:

$$V_{t,p} = \frac{\Delta H_{t,p}}{z_F F} \quad (2.23)$$

The temperature of electrolyte changes the voltages. In particular an increase of temperature would have a lowering effect on the enthalpic voltage. Regarding pressure, it has no significant effects on the enthalpic voltage [19].

The thermo-neutral voltage² V_{tn} is the voltage needed to make the cell work in thermo-neutral conditions, in which the heat need of the cell is matched with the heat generated by irreversibilities. The effect of thermodynamic parameters is much more relevant on the thermo-neutral voltage; an increase of temperature will effect the V_{tn} increasing it. Pressure will act in the reverse way; an increase of pressure will correspond in an decrease of the V_{tn} .

The parameters V_{tn} , and $V_{t,p}$ would be affected only by pressure and temperature, and also by the electrolyte concentration in the case of V_{tn} . They do not depend on the magnitude of electrolyzer current, consequently being almost independent from the hydrogen production rate [18]. Considering an ideal process, the enthalpic voltage equals the thermo-neutral voltage [16]. However, in a real electrochemical process $V_{tn} > V_{t,p}$.

²see next subsection for a more detailed description of the thermo neutral voltage and operation

2.2.1 Thermal behaviour of the cell and mode of operation

An electrochemical cell exchanges electrical and thermal power with the environment. Considering the thermal behaviour of the cell, the heat Φ is governed by two contributions: thermodynamics, the heat generated due to the electrochemical reaction Φ_{react} ; transport processes, the heat generation related to the irreversibilities of the transition processes Φ_{irr} .

Considering the cell operation in the electrolyzer mode, $\Delta\bar{g}_{react} > 0$. The first contribution of heat \bar{q}_{react} is positive and it is ruled by the entropy variation and temperature.

$$\bar{q}_{react} = T\Delta\bar{s}_{react} \quad (2.24)$$

It represents the heat power that need to be provided to the system. The behaviour is endothermic and the heat of reaction can be expressed as

$$\Phi_{react} = \frac{T\Delta\bar{s}}{zF}I \quad (2.25)$$

The second contribution Φ_{irr} is always exothermic because is related to irreversible processes³

$$\Phi_{irr} = I \sum_{j=1}^3 \eta_j \quad (2.26)$$

The figure 2.2(b) summarize the thermal behaviour of the electrochemical cell.

Considering the total heat as the sum of the two contributions and considering the sign of them, from 2.25 and 2.26:

$$\Phi_{cell} = \Phi_{react} - \Phi_{irr} \quad (2.27)$$

$$= \left(\frac{T\Delta\bar{s}}{zF} - \sum_{j=1}^3 \eta_j \right) I \quad (2.28)$$

Knowing from 2.17; the 2.27 become:

$$\Phi_{cell} = \left(\frac{\Delta\bar{h}}{zF} - \frac{\Delta\bar{g}}{zF} - \sum_{j=1}^3 \eta_j \right) I \quad (2.29)$$

and finally

$$\Phi_{cell} = \left(\frac{\Delta\bar{h}}{zF} - V_c \right) I \quad (2.30)$$

³The overvoltages η_j will be explained in the next paragraph 2.3

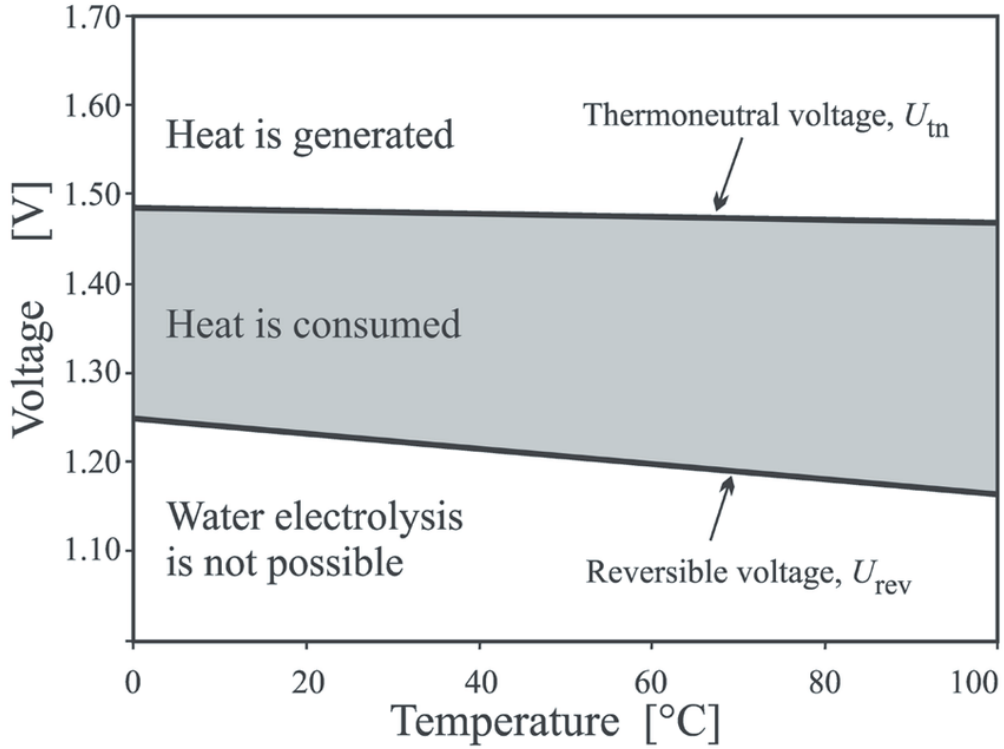


Figure 2.3: Reversible and thermo-neutral voltage behaviour, function of temperature at $p = 1 \text{ bar}$ [20].

From the figure 2.3 it is possible to observe the point of thermo-neutrality, which becomes a line in the temperature dependent graph. It divides the endothermicity zone from the exo-thermicity zone. The thermo-neutral point is defined by two fundamentals coordinates at a certain temperature; it is defined by the thermo-neutral current I_{tn} , while its projection on the y-axis permits to evaluate the thermo-neutral voltage V_{tn} , which is defined as

$$V_{tn} = \frac{\Delta \bar{h}}{zF} \quad (2.31)$$

at which correspond $\Phi_{cell} = 0$.

Considering that the standard enthalpy for water splitting is $\Delta H^0 = 286 \text{ kJ/mol}$, V_{tn} at standard condition corresponds to 1.482 V [11]. The value of the thermo-neutral current is affected by the operation temperature. At lower temperature the transport processes are more detrimental, resulting in a lower exchange current density (i_0) and higher air specific resistance, while the thermo-neutrality point moves at lower currents; at higher temperature the kinetics of the electrochemical reaction are improved and the thermo-neutrality point moves at higher currents.

In conclusion, the electrolyzer could work in three different conditions: endo-thermicity, exo-thermicity, thermo-neutrality. The decision over one instead of another depends on several parameters. The mode of operation could be always controlled handling the applied voltage.

2.2.2 Thermodynamic losses

Outside the thermo-neutral point, the electrolyzer operates in a non-thermal-balanced condition. Heat removal or supply management should be taken into account when considering the operations. In particular, the thermo-balanced voltage (V_{tb}) could be defined as [18]:

$$V_{tb} = V_{tn} + V_{conv} + V_{rad} \quad (2.32)$$

where V_{conv} and V_{rad} is the additional contribution of convection and radiation losses, respectively, to the overvoltage. V_{conv} and V_{rad} are not state function, so that neither V_{tb} is a thermodynamic state function. Convection losses could be estimated by the expression [21]:

$$P_{conv} = 1.77A(T - T_a)^{1.25} \quad (2.33)$$

where A is the heat transfer area, T_a is the ambient temperature. Correspondingly the radiation losses could be defined by the fourth-power law:

$$P_{rad} = A\epsilon\sigma(T^4 - T_a^4) \quad (2.34)$$

where ϵ is the emissivity, σ is the Stefan-Boltzmann constant. It should be noted that both V_{conv} and V_{rad} are inversely proportional to the imposed current, at fixed operating temperature. The voltages could be expressed as the power losses per unit of current.

2.3 Electrochemistry

When applying a DC current on the two end of an electrolyzer, the voltage of the cell experiences an increase, with the respect to the open circuit condition [16]. This phenomenon is mainly caused by different irreversible processes, such as overvoltages and parasitic currents, which generate energy losses limiting the cell efficiency. In order to maximize the hydrogen production with minimal amount of energy, it is important to understand all these phenomena affecting the operating voltage of an electrochemical cell. It is also necessary to investigate the effect of operating parameters and device design in the formation of overvoltages.

2.3.1 Polarization curve

The polarization curve expresses the relationship between current (I) and voltage (V_c) of the cell. It is fundamental for the comprehension of an electrolytic cell. Each curve is characteristic of temperature, pressure, and type of cell considered [22].

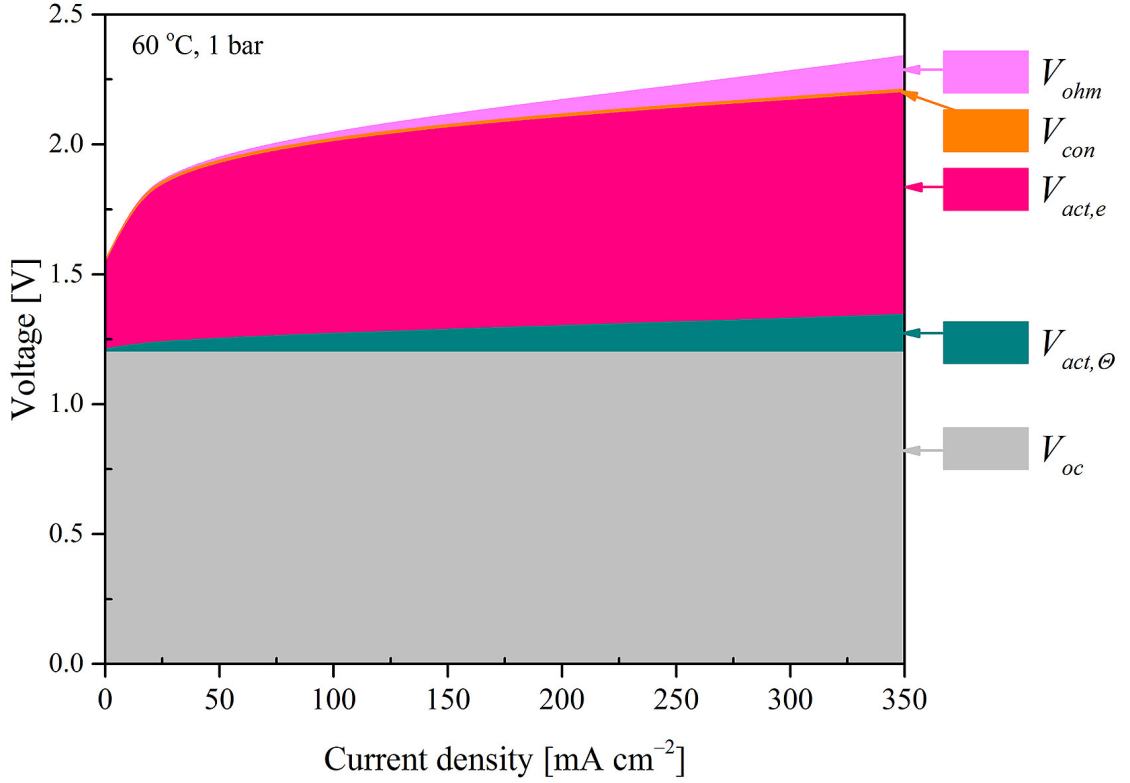


Figure 2.4: Polarization curve. The contribution of different irreversible phenomena is highlighted in different colors. $V_{act,\Theta}$ is the contribution from bubble coverage of the electrodes, while $V_{act,e}$ is the contribution from the bubble-free electrodes [23].

The cell voltage (V_c) increases with the respect to the reversible voltage (OCV), when a direct current (DC) is supplied to the electrochemical cell. This phenomenon is due to the insurgence of overpotentials related to irreversibilities in the process, which generate energy losses and limit the efficiency of the cell. The voltage of the cell is function of the current:

$$V_c = V_c(I) \quad (2.35)$$

it can be explicated as the sum of the open circuit voltage and three overpotentials

[16]:

$$V_c = OCV + \sum_{j=1}^3 \eta_j(I) \quad (2.36)$$

or more explicitly

$$V_c = \frac{\Delta \bar{g}_{react}(T, p_i)}{zF} + \eta_{act}(I) + \eta_{ohm}(I) + \eta_{diff}(I) \quad (2.37)$$

2.3.2 Transport phenomena

The electrochemical cell at open circuit is in its equilibrium condition and experiences the Nernst potential at its terminals. Closing the circuit, the electrochemical system goes out of equilibrium, and the physics will be dominated by transport processes; in particular by charge transfer, charge migration and a third phenomenon, mass transport; all of them affect the ideal voltage (OCV). These effects act in terms of degradation, generating entropy and modifying the voltage of the cell. The modification of voltage from the ideal one is called overvoltage (η). The charge transfer dominates low current operations with the generation of the activation overvoltage (η_{act}); the central part of the graph (2.4) is linear and dominated by charge migration and the ohmic overvoltage (η_{ohm}); in the final part of the graph (high currents) occurs the starvation of molecules, which should react with the catalysts; mass transport is prevailing, leading to the formation of diffusion overpotential (η_{diff}).

It is useful to normalize the current (I) by the area of the electrodes (S) in order to obtain the current density (i in A/m^2 or A/cm^2)

$$i = I/S \quad (2.38)$$

Activation overvoltage

Activation overvoltage is a phenomenon related to charge transfer processes that occurs in the electrodes oxidation and reduction. It is the energy needed to overcome the activation energy of oxygen and hydrogen formation reactions [24]. Due to the reaction nature of charge transfer, the activation overvoltage is dominated by kinetic effects. The kinetic law, in its general form, is expressed as:

$$k_R = k \cdot \exp[\beta n_{RDS} F \eta / RT] \quad (2.39)$$

where k_R is the current transferred; k is the rate constant, representing the current transferred when $\eta = 0$, i.e. at open circuit condition or equilibrium condition; β is the symmetry factor; n_{RDS} are the number of electrons transferred in the rate determining step. k is also called the exchange current (I_0), and it is characteristic of

the electrochemical reaction, of the type of electrode and catalyst and of temperature. Charge transfer process is regulated by a combination of forward (2.40) and backward (2.41) reactions:

$$k_{R,f} = k \cdot \exp[\beta n_{RDS} F \eta / RT] \quad (2.40)$$

$$k_{R,b} = k \cdot \exp[(1 - \beta) n_{RDS} F \eta / RT] \quad (2.41)$$

The resulting kinetic law is then:

$$k_R = k_{R,f} - k_{R,b} = k \cdot [\exp(\beta n_{RDS} F \eta / RT) - \exp((1 - \beta) n_{RDS} F \eta / RT)] \quad (2.42)$$

Explicating in favour of η :

$$\eta_{act} = \frac{RT}{\beta n_{RDS} F} \sinh^{-1}(I/2I_0) \quad (2.43)$$

or in terms of current density

$$\eta_{act} = \frac{RT}{\beta n_{RDS} F} \sinh^{-1}(i/2i_0) \quad (2.44)$$

where i_0 is the exchange current density. The anodic half-reaction produces a much higher activation overvoltage than the cathodic half reaction [16]. Another way to express the activation overvoltage is by means of a logarithmic behaviour. The Butler-Volmer equation give an accurate description of the activation phenomenon [25]. It is defined as:

$$\eta_{act} = \frac{RT}{\alpha_{anode} F} \ln\left(\frac{i}{i_{0,anode}}\right) + \frac{RT}{\alpha_{cathode} F} \ln\left(\frac{i}{i_{0,cathode}}\right) \quad (2.45)$$

where α_{anode} and $\alpha_{cathode}$ are the charge transfer coefficients for anode and cathode, respectively.

The activation overpotential could be further divided into two contributions [23]. The first effect is due to the presence of bubbles, which isolate part of the electrodes surface from the electrolyte, inactivating part of the area. The other contribution is due to the the activation current i_0 , previously described.

$$\eta_{act} = \frac{RT}{\alpha_{anode} F} \ln\left(\frac{i}{i_{0,anode}(1 - \Theta_{anode})}\right) + \frac{RT}{\alpha_{cathode} F} \ln\left(\frac{i}{i_{0,cathode}(1 - \Theta_{cathode})}\right) \quad (2.46)$$

Ohmic overvoltage

Charged species rule the behaviour in the central part of the polarization curve. They create a linear increase of the voltage with the current increasing, called ohmic overpotential η_{ohm} . It is a phenomenon related to the ohm law of electron and ionic species.

$$\eta_{ohm} = RI = ASR \cdot i \quad (2.47)$$

where R is the resistance of the conductor; ASR is defined as the area specific resistance in $[\Omega m^2]$ and is equal to the product between the length of the conductor pathway (L) and the resistivity of the conductor (ρ): $ASR = \rho L$. More in detail the ohmic overpotential could be expressed as

$$\eta_{ohm} = (\rho_{e^-} L_{e^-})i + (\rho_{ion} L_{ion})i \quad (2.48)$$

The total electrical resistance is function of different contribution: electrolyte resistance, membrane resistance, bubbles resistance and circuit resistance⁴.

Diffusion overvoltage

The diffusion overpotential depends on two parameters of the cell: the concentration at the bulk (C_{bulk}) and the concentration at the cathode (C_{cat}). It is defined as the activation energy required to drive mass transfer, at the rate needed to support the current [26]. In order to properly address the problem, it is necessary to use a transport model from the various existing in literature [27, 28]:

- Fick's law is the simplest model, which performs well with the mixture of two components [29]
- Stefan-Maxwell model could be used for multicomponent mixtures
- Dusty-gas model account for the Stefan-Maxwell model and the Knudsen diffusion, in porous media [30]

If using the Dusty-gas model, measuring the concentration at the bulk and calculating the concentration at the cathode, the calculation of the OCV will take into account the concentration effect and will be no more necessary the η_{diff} term in the polarization equation 2.37.

However, for the other cases, the diffusion overpotential will be described. At high current densities the cell will experience a starvation of molecules available for reaction in the catalyst. This phenomenon is deleterious for the performances and,

⁴The different resistance contribution will be explained in detail in the next paragraph 2.3.3

at the same time, it is degrading for the catalyst material, that starts to oxidize. Applying the simplest Fick's law:

$$\frac{\dot{n}_i}{s} = D_{eff,i} \nabla c_i \quad (2.49)$$

where D_{eff} is the diffusion coefficient as a correction of the diffusion coefficient in the bulk

$$D_{eff,i} = \epsilon D_{i,BULK} / \tau$$

in which ϵ is the porosity of the solid matrix composing the electrode, τ is the tortuosity of the electrode, characteristic of the matrix and of the type of molecule. Simplifying into the mono-dimensional case, 2.49 become:

$$\frac{\dot{n}_i}{s} = D_{eff,i} \frac{dc_i}{dx} \quad (2.50)$$

and approximating the derivative

$$\frac{\dot{n}_i}{s} = D_{eff,i} \frac{C_{BULK} - C_{CAT}}{t} \quad (2.51)$$

where t is the thickness of the electrode. Considering the correlation between \dot{n}_i and current exchanged on the electrode 2.8

$$i = \frac{D_{eff,i}(C_{BULK} - C_{CAT})_i}{z_i F t} \quad (2.52)$$

A limit arise for $C_{CAT} \rightarrow 0$ creating the concept of limiting current density:

$$i_l = \frac{D_{eff,i} C_{BULK,i}}{z_i F t} \quad (2.53)$$

Finally the diffusion overpotential could be calculated as the difference between the concentration at the bulk and the concentration at the catalyst [23]:

$$\eta_{diff} = OCV(C_{CAT}) - OCV(C_{BULK}) \quad (2.54)$$

$$= \frac{RT}{zF} \ln C_{CAT} - \frac{RT}{zF} \ln C_{BULK} \quad (2.55)$$

$$= \left| \frac{RT}{zF} \ln(C_{CAT}/C_{BULK}) \right| \quad (2.56)$$

absolute values are added in order to make the overpotential non-negative. The expression 2.54 explains that the diffusion overpotential is a correction parameter, that account for the concentration of the cathode, only when the concentration at the bulk is known. Considering 2.52 and 2.53:

$$\eta_{diff} = \left| \frac{RT}{zF} \ln(1 - i/i_l) \right| \quad (2.57)$$

Considering alkaline electrolysis the value of the diffusion overpotential is much lower than η_{ohm} and η_{act} [16].

The expression of the polarization curve for a cell operating with $\Delta g > 0$ will be:

$$\begin{aligned}
 V_c = & + \frac{\Delta \bar{g}_{react}(T, p_0)}{z_F F} + \frac{RT}{z_F F} \ln \frac{\prod^P (C_{P, BULK})^{\nu_i}}{\prod^R (C_{R, BULK})^{\nu_i}} \\
 & + \left[\frac{RT}{\beta n_{RDS} F} \sinh^{-1}(i/2i_0) \right]_{anode} + \left[\frac{RT}{\beta n_{RDS} F} \sinh^{-1}(i/2i_0) \right]_{cathode} \\
 & + ASR \cdot i \\
 & + \left[\left| \frac{RT}{z_F} \ln(1 - i/i_l) \right| \right]_{anode} + \left[\left| \frac{RT}{z_F} \ln(1 - i/i_l) \right| \right]_{cathode} \quad (2.58)
 \end{aligned}$$

2.3.3 Electrical circuit analogy

There are barriers to overcome, in order to make the electrochemical reaction process to advance. The various overpotentials could be expressed also doing a reference to the electrical circuit theory. In particular the ohmic overvoltage could be expressed as a total ohmic resistance $\sum R$ expressed as:

$$\sum R = R_{ions} + R_{membrane} + R_b + R_c \quad (2.59)$$

where R_{ions} , $R_{membrane}$, R_b and R_c are electrolyte resistance, membrane resistance, bubbles resistance and circuit resistance, respectively. R_{ions} could be minimized by increasing the concentration of conductive salts. However, the concentration of KOH or $NaOH$ is about 20% – 35% for alkaline electrolyzers, because a further addition of salt would result in an excessive corrosion of the cell and destruction of the membrane [31]. $R_{membrane}$ and R_c could be minimized by optimizing the wire connections and production process of the membrane. R_b is a more complex term generated by the covering of the electrodes surface by oxygen and hydrogen bubbles that will reduce the conductivity⁵.

More specifically the resistances seen could be further divided as in fig. 2.5. Where R_c is split in two terms accounting for the external electrical circuit resistance including wiring and connections at anode (R_1) and at cathode (R'_1). The resistance of electrodes is divided in two resistances in series for anode R_{anode} , originated from the overpotential of the oxygen evolution reaction, and cathode $R_{cathode}$, caused by the overpotential for the hydrogen evolution reaction. R_b is different between the anode and cathode and is accounted as R_{bubble, O_2} for specifying the resistance due to partial coverage of the anode and R_{bubble, H_2} for the resistance due to partial

⁵Bubble effect and improvement methods will be studied separately in the next section 2.4.

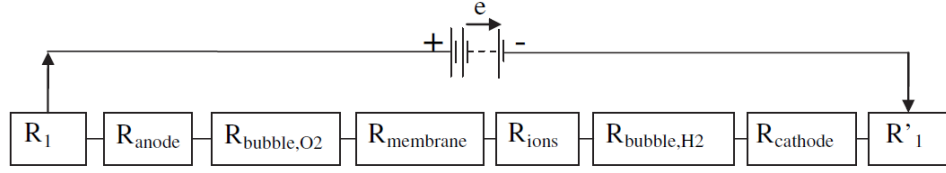


Figure 2.5: Complete electrical circuit analogy of resistances in the water electrolysis system [32].

coverage of the cathode with hydrogen bubbles. Finally $R_{membrane}$ and a further resistance R_{ions} are introduced to specify the membrane and electrolyte resistance respectively. All these resistances could be classified into three categories: electrical resistances; transport-related resistances; electrochemical reaction resistances. Circuit resistances R_1 and R'_1 belong to the first category of electrical resistances and can be calculated from the Ohm's second law: $R = L/(kA)$, where L is the length of the conductor, k is the specific conductivity, and A is the cross-sectional area. Transport-related resistances are the physical resistances experienced in the electrolysis process, R_{bubble,O_2} , R_{bubble,H_2} , R_{ions} and $R_{membrane}$ belong to this second category. Finally R_{anode} and $R_{cathode}$ are reaction resistances. These resistances arise due to the overpotentials required to overcome the activation energies of hydrogen and oxygen formation reactions on the electrodes surface.

2.3.4 Efficiency evaluation

Usually, energy efficiency is expressed as the ratio between the energy output versus the energy input. However, different efficiencies could be defined and evaluated for an electrolysis cell, depending on the purpose:

- Voltage efficiency. It represents a good approximation of the electrolyzer efficiency. Voltage efficiency can be calculated as the difference between voltage of anode and cathode normalized by the cell voltage [33].

$$\eta_{voltage} = \frac{(V_{anode} - V_{cathode})100}{V_c} \quad (2.60)$$

It physically represents the proportion of the effective voltage needed for the water splitting process toward the voltage applied at the electrodes terminals.

- Faraday efficiency. It uses the Gibbs free energy change of water decomposition reaction as the energy input [32].

$$\eta_F = \frac{\Delta G}{\Delta G + Losses} \quad (2.61)$$

The Faraday efficiency could also be expressed in voltage terms as:

$$\eta_F = \frac{V_{\Delta G}}{V_c} \quad (2.62)$$

$V_{\Delta G}$ is the equilibrium voltage. The physical meaning of faradic efficiency is the percentage of the theoretical energy needed to force apart the water molecules in the real cell voltage.

- Thermal efficiency. Similarly to the Faraday efficiency, it uses the entalpy change of water decomposition reaction as the energy input [32].

$$\eta_{Thermal} = \frac{\Delta H}{\Delta G + Losses} \quad (2.63)$$

Thermal efficiency could also be expressed in voltage terms as:

$$\eta_{Thermal} = \frac{V_{\Delta H}}{V_c} \quad (2.64)$$

$V_{\Delta H}$ is the thermo-neutral voltage. It is possible to obtain thermal efficiencies over 100% when the system operates in endothermic mode (absorbing heat from the environment). In physical terms, equation 2.64 means that, it requires an additional cell voltage in order to maintain the thermal balance.

- H_2 production rate efficiency. It express the hydrogen production rate per unit electrical energy input [32].

$$\eta_{H_2productionrate} = \frac{f_{H_2productionrate}}{\Delta E} \quad (2.65)$$

where $f_{H_2productionrate}$ is the production rate of hydrogen⁶

- HHV efficiency. It represents the high heating value (HHV) of one mole of hydrogen over the energy input [32].

$$\eta_{HHV} = \frac{HHV_{H_2}}{\Delta E} \quad (2.66)$$

- Net efficiency. Energy efficiency could be expressed also in terms of losses over the input [32].

$$\eta_{net} = 1 - \frac{E_{loss}}{E_{input}} \quad (2.67)$$

where E_{loss} are the sum of all the energy losses caused by overpotentials discussed previously (subsection 2.3.3).

⁶see subsection 2.3.5 for the definition of the hydrogen production rate

Factors that influences the efficiency

Many factors affect the efficiency. In order to reduce the electricity consumption of electrolyzers as much as possible, it is important to understand the optimal parameters configurations which maximize the efficiency. As known, the voltage of the cell depends on the open circuit voltage, function of the type of reaction, and the sum of overvoltages caused by irreversible processes. Factors that are discussed below affect the overvoltages, consequently affecting the final efficiency of the electrochemical cell [34]. It is possible to reduce the splitting energy, reducing the decomposition voltage by increasing temperature or changing reaction process [31]. A bigger number of factors influences the overpotentials, they are:

- Electrolyte quality: salt is needed to make the water conducting electrons, but a concentration limit exists because of corrosion effect on involved components, reducing their lifetime. The existence of impurities, inside the electrolyte solution, makes the ohmic resistance increase, due to the blocking and passivation effect on electrodes/membrane surfaces.
- Temperature: splitting reaction potential of water reduces as temperature increases [35], which will correspond in a lower reversible potential with the respect to standard conditions. In addition, surface reaction and ionic conductivity of an electrolyte are expected to be raised with temperature [36]. Higher temperature corresponds to a lower voltage required to drive electrolysis, and therefore in a lower energy for the same amount of hydrogen produced. However another effect is an increase of the gas bubbles size and the reduction of their rising velocity.
- Pressure: increasing the pressure reduces the amount of required power because the diameter of bubbles will be reduced. It also reduces the amount of required power for further compression of the gases, becoming particularly advantageous in case of needing pressurized products [37]. However, it should be noted an increase in the total energy consumption of the system, due to the pressurization of water.
- Electrical resistance: the ohmic contribution in the cell voltage depends mainly on distance between electrodes, size and alignment of electrodes, forcing the bubble removal⁷. Ions start their travel on the surface of the cathode and reach the anode, passing through the electrolyte and the separator. Reducing the distance between the two electrodes will help reducing the ohmic resistance, however an excessive reduction could cause a less efficient process, due to the

⁷For more detailed description of gas bubble effect see section 2.4

the increase of the void fracture. Another factor was observed in the cross section area; the vertical alignment is the best choice to achieve an optimal bubble departure [38]. It was also observed that a high accumulation of bubble in the upper part of electrodes, creates a higher void fraction leading to an increase in the potential needed by the cell. The ohmic resistance revealed to be proportional to the bubble coverage of electrode; using strategies, to force bubbles to leave, could be considered a way to optimize the cell efficiency.

- **Electrode material:** materials employed interact with the electrochemical behaviour of the cell. The main differences consist in the level of activity, resistivity against corrosion and lifetime⁸. Porous sintered electrodes shows an higher activity compared to smooth one; the increased exposed surface area is the reason [34].
- **Separator material:** the presence of a separator increases the accumulation of the bubbles around electrodes, increasing the void fraction. The materials employed should minimize this negative effect; a popular material in 90s was asbestos that showed to be toxic and hazardous, so that it is replaced nowadays with safer solutions.

2.3.5 Specific energy consumption

It is possible to write the theoretical specific energy consumption related to an electrolysis process, expressed in $[kWh/Nm^3_{H_2}]$ as function of the voltage of the cell, of the current and of the time:

$$E_{sp} = I \cdot t \cdot V_c(i) = Q \cdot V_c(i) \quad (2.68)$$

According to Faraday's law, the electric quantity (Q) to produce 1 *mol* of H_2 (i.e. 22.4 *l* at standard condition) is $2 \cdot F$ [31]. Therefore

$$E_{sp} = \left(2 \cdot \frac{1000}{22.4} \cdot 96485 \cdot \frac{1}{1000} \cdot \frac{1}{3600}\right) \cdot V_c(i) \quad (2.69)$$

Considering now the case of water electrolysis, it is possible to identify a lower value for the energy required per Nm^3 of H_2 produced. Considering standard conditions, $T = 25^\circ C$ and $p = 1bar$, it is possible to evaluate the standard Gibbs free energy of the reaction (2.1). From equation 2.20 it is possible to calculate the equilibrium potential of the water electrolysis process that will be:

$$OCV = \frac{\Delta\bar{g}(T, p)}{2F} = 1.23V \quad (2.70)$$

⁸Refer to section 2.5 for a comparison between the most employed electrodes materials

This value corresponds to the minimum value of voltage to be applied for water decomposition. Finally

$$E_{sp}(STP) = 2.39 \cdot 1.23 = 2.94 kWh/Nm^3_{H_2} \quad (2.71)$$

which is the minimum amount of energy to be spent to split water at STP. However different dissipation processes reduce the efficiency of the device, causing a variation in the real voltage of the cell that always needs to be higher than the ideal one, and it is furthermore function of the current density; the real specific consumption will change with the type of electrolyzer considered and the parameters of operation. Practical cell voltage are far over $1.23 V$, reaching about $1.8 - 2.6 V$ in industrial cells for water electrolysis [31].

In order to relate the energy consumed to the hydrogen produced in a real process, it is important to define the hydrogen production first; hydrogen production rate f_{H_2} [Nm^3/h] is defined as [16]:

$$f_{H_2} = \eta_F \frac{N_{cell} I_{cell}}{zF} \frac{22.41}{1000} 3600 \quad (2.72)$$

where η_F is the Faraday efficiency⁹, N_{cell} is the number of cells that constitute the electrolysis module, and I_{cell} is the cell's current in A. The previous formula is valid only under the assumption of hydrogen as an ideal gas.

The specific energy consumption usually increases with the production rate [22] and can be calculated as follows:

$$E_{sp} = \frac{\int_0^{\Delta t} N_{cell} \cdot I_{cell} \cdot V_c dt}{\int_0^{\Delta t} f_{H_2} dt} \quad (2.73)$$

The previous expression is only related to the electrolysis process, it does not consider energy consumption of auxiliary system and equipment that may be present in a real hydrogen production system, such as magnetic valves, sensors, microprocessors, electrolyte cooling systems, and purification units. It neither includes the losses related to the electric power supply. All these sources of additional energy consumption should be taken into consideration when addressing the specific energy consumption of the global production facility.

2.3.6 Specific water consumption

Another important parameter to evaluate is the specific water consumption. It is possible to calculate it from stoichiometric consideration. Always referring to the

⁹The Faraday efficiency, also known as current efficiency, is defined in section 2.3.4

reaction (2.1), it is possible to state that 1 mole of hydrogen is produced every mole of water. Considering the molecular weight of water $MM_{H_2O} = 18.015 \text{ g/mol}$ [39] and the molecular weight of hydrogen $MM_{H_2} = 2.016 \text{ g/mol}$ [40], every 8.936 *kg* of water will be able to transform into 1 *kg* of hydrogen. Considering now the densities of the compounds ($\rho_{H_2O} = 1 \text{ g/L}$ and $\rho_{H_2} = 0.08988 \text{ g/L}$), it is possible to define the specific water consumption as the density ratio between water and hydrogen

$$C_{H_2O} = \frac{V_{H_2}}{V_{H_2O}} = 0.8988 l_{H_2O} / Nm_{H_2}^3 \quad (2.74)$$

This kind of parameter is very important during the design stage of an electrolyzer project, because it is needed for the assessment of a water supply facility nearby the plant.

2.4 Advanced alkaline solution

In this section the main problems regarding water electrolysis systems will be discussed. Possible solutions will be also proposed as advanced alkaline systems. Firstly, the issues related to the produced gases will be described. Later, on the section, the problem related to bubbles will be presented; the detrimental effect on the electrolyzer efficiency will be discussed. At the end, some actions to enhance water electrolysis will be proposed, limiting the bubbles negative effect.

2.4.1 The problem of bubbles

The water splitting reaction, driven inside the electrolysis cell, creates the gaseous product O_2 and H_2 from the liquid H_2O . These products are generated in proximity of the electrodes, at the anode and at the cathode respectively, with the main effect of reducing the effective active area for the reaction [41]. Bubbles grow gradually in time, and leave the surface when a certain size is reached. The covering of the electrode surfaces could be seen as an increasing of the ohmic resistance, due to the reduced contact between the electrodes and electrolyte, with the consequence of blocking the electron transfer [32]. Bubbles move to the top of the AEL cell, where a froth layer is formed. The thickness of the froth layer increases with the height [31]. The void fraction is the main parameter to describe the bubble effect; it is influenced by solution composition, pressure, current density, bubbles size, bubbles layer thickness and electrode spacing. Understanding and minimizing the bubble effect is necessary in order to enhance the electrolyzer efficiency.

2.4.2 Ways to enhance water electrolysis

The bubbles size affects the detachment rate and so the electrolysis specific energy consumption. However other factors could influence the bubbles disengagement such as surface tension and attractiveness of electrode surface. In literature, different solutions are proposed in order to reduce the deleterious effect of bubbles [31].

Apply an external field

The application of external field could help the bubbles prematurely leave the surface of electrodes. A magnetic field could be imposed in order to decrease bubbles coverage and void fraction. The magnetic effect is more effective shortening the inter-electrodes distance. Ultrasonic field helps in the detachment process. It helps to promote mass transfer, especially at high current density and lower electrolyte concentration. The collapse of cavitating bubbles, formed under the ultrasonic field, generate chaotic flows accelerating the bubbles disengagement. Super gravity fields represent another solution. It acts on the buoyancy, the actual driving force for bubbles detachment.

Adopt new electrolyte composition

Another way to reduce energy consumption for water electrolysis is to add ionic activators in the electrolyte. It represents an efficient method to solve the bubbles issue, due to low cost and simple operation. Surfactants are another additive able to adjust the wettability of electrodes. Using ionic liquid/water electrolyte could be an alternative promising solution, also corrosionwise [42]. They exhibit good conductivity and they are chemical inert to metal electrodes [43].

Adopting new system for water electrolysis

Another way to reduce the bubble effect is to act on the thermodynamic decomposition voltage. A promising method could be that of using new systems as solid oxide electrolysis cells. This kind of electrolyzers work at higher temperatures with a different reaction route, reducing the decomposition voltage, increasing the efficiency¹⁰.

2.4.3 Safety issues

One of the main issue, of water electrolysis in general, is the formation of hazardous gases. Oxygen and hydrogen are highly reactive gases, that must be treated

¹⁰Refer to chapter A for a more detailed description of SOEC

carefully to avoid explosion hazards. In particular a limitation on the gas crossover is imposed to not overcome the lower explosion limit of the gases [44]. The LEL and UEL of hydrogen is of 3.8 *mol%* and 95.4 *mol%* respectively, at atmospheric pressure and 80°C [45]. A usual safety limit for commercial electrolyzer is imposed at almost half of LEL, equal to 2% H_2 concentration in O_2 [46]. Gas composition measuring system must be installed for live monitoring of produced gases, and an emergency switch down of the electrolyzer must be imposed when the H_2 overcome its limit value in the anode side. A source of contamination is represented by the product gases diffusion, through the separator. This will make part of the oxygen to react back with hydrogen into water, reducing the electrical efficiency of the process. Dissolution of gases, in the electrolyte solution, represents another contamination effect. The poisoning demonstrated to be relevant at low current density, and consequently at low hydrogen production rate. This problem could be considered significant when the electrolyzer is coupled with renewable generators; part load operations are more probable and must be controlled to not go below 10% – 40% of the nominal load [47]. A proposed solution in literature it is that of using platinized current collectors, where hydrogen could catalytically react with oxygen [48]. The proposed model for gas impurities has the aim of predicting the gas crossover. The hydrogen in oxygen content (HTO) is modeled depending on the current density, the temperature and pressure of operation. The influence of each parameter on the gas purity is discussed.

2.5 Materials employed in alkaline electrolyzer and design

An alkaline water electrolysis cell is composed of four main components: the electrodes, the electrolyte solution and the diaphragm. The balance of the plant account for all those components needed for the appropriate functioning of the system.

2.5.1 Electrode materials

Electrodes differ in cathode and anode, where hydrogen and oxygen separate, respectively. The cathode represents the direction of flow of positive charges and it is the electrode at which reduction reaction occurs. In the electrolyzer mode of operation (electrical power provided to the device), the cathode is the negative pole, while the anode is the positive one. Materials employed for the cathode could be divided in classes based on their overpotential: metals with high overpotential, such as *Cd*, *Ti*, *Hg*, *Pb* etc.; metals with middle overpotential, like *Fe*, *Co*, *Ni*, *Cu* etc.; metals with low overpotential as *Pt* and *Pd* [49]. Same materials could

be employed also for the anode; the most common material is *Ni* and its alloys, at present [49].

2.5.2 Electrolyte materials

The electrolyte used in alkaline systems are aqueous solution of *KOH* or *NaOH*, and more rarely *H₂SO₄* [49]. These salts are dissolved in demineralized water in order to increase the conductivity of the liquid solution, reducing the ohmic losses. However, these solutions can have corrosive behaviour on the electrodes, reducing the catalytic activity and the cell lifetime. In order to reduce the corrosive nature of the electrolytes, *BIMBF₄* molecular electrocatalyst could be added. To maximize the ionic activation some additives could also be included in the solution. The most popular is the *Na₂MoO₄*, *Na₂WO₄* ethylenediamine based metal chloride complex. In this way the energy requirements for water splitting could be reduced.

2.5.3 Diaphragm materials

The role of the diaphragm is to avoid the mixing of the produced gases, between cathode and anode; it provide insulation between the electrodes of opposite polarity, preventing any short circuit. More specifically, a separator must show a low resistance, a low *O₂* content in *H₂* (low cross contamination of generated gases) and high durability [50]. Asbestos was the main material, employed until '90s because of its wettable property and highly porosity structure which results in a low electrical resistance [51]. However, nowadays it is known to be a toxic and hazardous material; it is no more employed in the electrolyzers' industry [52]. Nowadays composite ceramic or microporous materials are used; polyethersulfone (*PES*) and glass reinforced polyphenylene sulfide (*PPS*) compounds are examples [49].

2.5.4 Balance of the plant

The balance of the plant includes all the equipment needed to operate the stack; such as, deionised water supply, heat exchangers, gas-liquid separator vessels, circulation pumps and the cooling loop. Other system requirements consist in power conditioning system, cooling water recirculation system, filtering structures [19].

2.5.5 Electrolyzer design

Water electrolyzers can be grouped into two classes depending on the cell configuration: unipolar and bipolar. The unipolar structure consist in electrodes carrying

the same charge on both faces. The electrodes, with the same sign, are connected in parallel in order to have the voltage of the stack equal to the voltage of a single cell. The hydrogen production could be raised by increasing the number of the electrodes, increasing the total current. The main advantages consist in simple construction, high reliability and great flexibility in operation. The low operational voltage is a pro for safety [19]. Bipolar design is most employed in modern alkaline electrolyzers. In this case electrodes are bipolar plates, working as cathode on one side and as anode on the opposite side. It consist of a series electrical connection, with the stack voltage depending on the number of cells. The individual cell is constituted by a pair of electrodes and the diaphragm. The bipolar configuration permits a more compact design and shorter current paths, reducing internal ohmic losses ; however, the presence of parasitic currents, could create corrosion problems [11]. Examples of these two configurations are showed in fig.2.6.

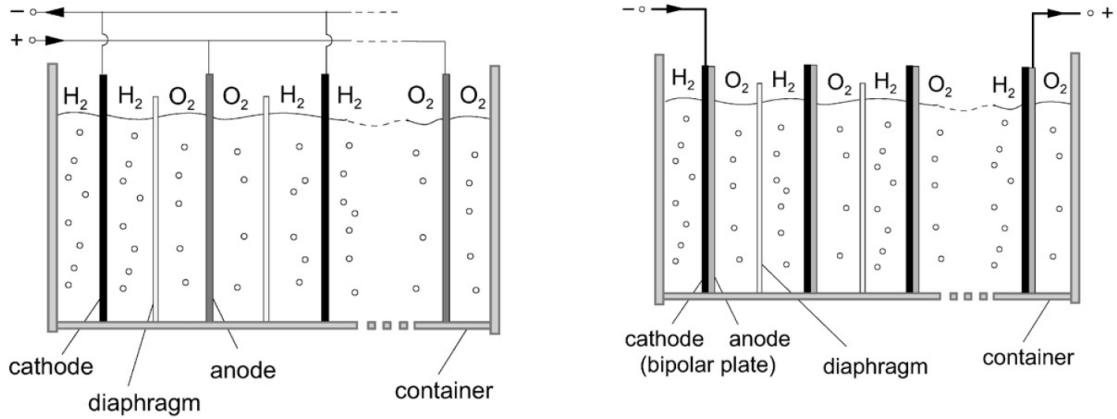


Figure 2.6: Unipolar (on the right) and bipolar (on the left) cell configuration [11].

Different electrolyzers architectures are proposed nowadays to reduce losses, improving efficiency and reducing energy consumption. The spacing between anode, diaphragm and cathode is a source of losses, due to ohmic phenomena. A zero-gap design would be preferred in order to reduce at minimum the spacing between the fundamental components, reducing the cell voltage [50]. This kind of configuration represents the state of art in modern alkaline electrolyzers [49]. This structure differs from the immersed electrode design, in the fact that the gas bubbles cannot create in the intra-electrode space. A new solution consist of having gas diffusion layers between the *Ni* net electrodes and the gas compartments [53]. This will make the gas cross-contamination more difficult, showing positive effects on the outlet gas purity.

2.6 Future efforts

In recent years more efforts are concerned on those fields, in which more deep understanding of processes and effects is needed [54]. Specifically, particular research attention is focused and will focus, on:

- Development of advanced electrocatalyst in terms of materials and design, in order to promote the electrolysis reaction, lowering the contribution of overvoltage due to activation [55]. Electrocatalysts are important for enhancing and establish the electrode activity. Also the research of new type of electrodes or electrode coatings should be addressed, in order to minimize deactivation phenomena.
- Optimal cell design in terms of minimization of the distance between electrodes, in order to reduce the ohmic resistance (lower ionic path) and increasing the maximum current density, increasing the hydrogen production [56].
- Development of new exchange inorganic membranes, for substituting liquid electrolytes; this would help reducing the mixing of produced gases, enhancing the ionic conduction at the same time [57].
- Characterization of the behaviour of electrolysis cells, by means of modeling the cell voltage and hydrogen production, as function of current density.
- Improved bubble management strategies are needed, to enhance the detachment of bubbles and reducing their electrode deactivation ability [32]. Gas bubbles are responsible of the increase of the ohmic losses. Study of mechanism and the development of a mathematical model could be future research topics to minimize this deleterious phenomenon.

Chapter 3

Mathematical modeling

Mathematical modeling of phenomena is used to describe and reproduce their characteristic behaviour under varying operating conditions. In this case a mathematical model is proposed for the characterization of a complete alkaline water electrolysis system for the hydrogen production. The model is first defined on Matlab, in which it is evaluated for the influence of the variation of working parameters. Finally the complete system is created on Aspen Plus, in which the model is implemented in the workflow of components.

In literature, different types of model employing different programs are proposed, in order to model the behaviour of an electrolyzer. Models could be divided into physical model and semi-empirical model. The physical ones could be further divided into multi-physics approach or mono-dimensional approach. Hammoudi et al. in [58] proposed a multi-physics approach for the modeling of a water alkaline electrolyzers. The main advantages of this model consist in the shorter time needed for the characterization of the parameters, compared to semi-empirical models, and in the fact that it could be extended to a range of alkaline electrolyzers. The cell voltage is described by means of physical relationship, in [59]. The aim of the work is to describe the electrical energy consumption at different current production and at different operative pressures. The variation from the ideal cell voltage is described by means of the activation overpotential, defined by means of the Butler-Volmer equation (2.45), by the ohmic losses and by the leakage current. A similar method is described in the loss-estimate approach in [60]. It characterizes the cell behaviour, considering the activation and ohmic losses. A reduced-order approach is also proposed, in order to simplify its implementation in complex system, as in electrolyzer plants coupled with storage and intermittent renewable generators. The same article also describes an equation for estimating the partial pressure of water, in order to derive the deviation from the perfect gases hypothesis. David et al. in [61, 62] developed a phenomenological based semi-physical model for a self-pressurized electrolyzer. The advanced description of the phenomena

involved are carried out for the cathode and the anode separately. The model is able to describe the dynamic responses to variation in the electrolyte concentration, allowing the prediction of the operational variables. An electrical static dynamic modeling is proposed by Ursua in [63]. The model is based on thermodynamics, activation, ohmic and double layer phenomena. The Matlab implemented model describes the dynamic cell behaviour in order to better characterize the coupling of the electrolyzer with renewable energy sources. A one-dimensional model in Simulink is proposed in [23]. Also in this case the advantage of the model consists in the applicability to different alkaline electrolyzer cells. The model is built using three different modular components (ancillaries): anode, cathode and voltage; it permits to understand the different contributions affecting the cell voltage. Semi-empirical models are the most diffused in literature; they consist in the description of the electrolyzer cell's behaviour, by means of operational parameters, calculated in the experimental phase. For this category, the paper by Ulleberg [11] might be considered of special interest. He describes a model as a combination of fundamental thermodynamics, heat transfer theory, and empirical electrochemical relationships. Every successive study, uses this article as starting point, because it permits to describe the electrochemical cell's behaviour with the use of only 6 inputs parameters. The extrapolation of the employed parameters is done from experimental data with curve retrofitting procedure. The detailed Matlab regression procedure is well described in [17]. In the same article, Amores et al. extend the Ulleberg's model, which depends only on temperature, to the effects of electrolyte concentration and cell architecture. In particular they proposed the existence of an optimal distance between electrodes, and the linear dependence of the ohmic resistance to this distance; also the electrolyte concentration was demonstrated to have an optimal value for the maximum conductivity, dependent on temperature with a quadratic relation. Other authors, Sanchez et al. in [54, 64, 65], proposed an enlarged mathematical relationship to highlight the dependence of the polarization curve from the temperature and pressure. The model was implemented in Aspen Plus using a sub-routine, Aspen Custom Modeler (ACM), for the implementation of the electrochemical equations. It considers also the impurity present in the generated gases, of particular importance for safety reasons; an emergency shutdown must be imposed in commercial electrolyzers when a content of 2 vol% foreign gas is measured in the exhaust, which is about 50% of the lower explosion limit (*LEL*) [44]. Diéguez et al. in [66], elaborated the concept of thermal modeling, focusing on the evolution of the electrolyzer temperature with time; the study is particularly interesting in the case of the coupling of the electrolysis system with a renewable energy plant. A similar approach is used in [67], where the thermal model is developed considering the effect of all sources of heat entering and exiting the system; from the definition of the heat accumulation speed is possible to determine the temperature rise speed. The possibility to get the time required for the alkaline

electrolyzer to reach the target temperature is of particular relevance for dynamic operation evaluation. The application of a model to a real, power variation example is evaluated in [68]. Finally [69] proposed a specific power consumption relationship, based on the amount of salt dissolved in the electrolyte and on the electrolyte density. All of these studies are analyzed and compared in order to get a new model, able to describe the alkaline electrolysis process in a comprehensive way; the effect of several operational parameters will be accounted for. The model will be characterized in Matlab for an initial calibration and verification. Then it will be exported in Aspen Plus in order to account also for the effect of the auxiliaries and all the system components. A table showing the main innovations of the present model is showed 3.1.

Table 3.1: Comparison table for different models. Starting from left: Ulleberg [11], Sànchez [64, 65], model proposed in this thesis.

| Characteristics | Ulleberg | Sànchez | Present model |
|------------------------|----------|---------|---------------|
| T dependent parameters | × | ✓ | ✓ |
| P effect | × | ✓ | ✓ |
| Thermal model | ✓ | × | ✓ |
| T transient behaviour | ✓ | × | × |
| Ion formation | × | × | ✓ |

3.1 Electrochemical model

Kinetics of an electrolyzer could be modeled using different empirical relationship describing different polarization curves. Several parameters could influence the functioning, therefore the I-V curve, of an alkaline electrolyzer. The greatest effect is the variation of the operational temperature, but will be accounted also for the effect of pressure, concentration of the electrolyte and distance between the electrodes.

3.1.1 Polarization behaviour

The expression of the voltage of the cell dependent from temperature is firstly described by Ulleberg [11] as:

$$V_c = OCV + r \cdot i + s \cdot \log(t \cdot i + 1) \quad (3.1)$$

Three main parameters could be observed in the equation. The *OCV* is firstly calculated in operative condition using the Nerst equation 2.20. The second

addendum specifies the effect of the ohmic resistance on the curve with varying the current density (parameter r). The effect of the diffusion overvoltage, previously explained, is here neglected. The last term relates to the effect of the activation overpotential, with the overvoltage coefficients s and t . The effect of the temperature is considered taking into account the parameters definition:

$$r = r_1 + r_2 \cdot T \quad (3.2)$$

$$t = t_1 + t_2 \cdot T + t_3 \cdot T^2 \quad (3.3)$$

The open circuit voltage at operative conditions is calculated considering the effect of temperature and pressure in two separated terms.

$$OCV = OCV^0 + \frac{RT}{zF} \ln\left(\frac{(p - p_{H_2O})^{1.5} p_{H_2O}^*}{p_{H_2O}}\right) \quad (3.4)$$

Where OCV^0 is the standard potential, p is the operative pressure, p_{H_2O} is the partial pressure of the wet hydrogen and oxygen gases near the electrode, $p_{H_2O}^*$ is the vapor pressure of pure water. The reversible potential for a given temperature at given pressure is calculated according to [58]:

$$OCV^0(T) = 1.50342 - 9.956 \cdot 10^{-4} \cdot T + 2.5 \cdot 10^{-7} T^2 \quad (3.5)$$

The effect of pressure is determined according to partial pressure equations [18].

$$p_{H_2O}^* = T^{-3.4159} \exp(37.043 - 6275.7/T) \quad (3.6)$$

and

$$p_{H_2O} = T^{-3.498} \exp(37.93 - 6426.32/T) \cdot \exp(0.016214 - 0.13082m + 0.1933m^{0.5}) \quad (3.7)$$

with the effect of electrolyte molality:

$$m = w \frac{(183.1221 - 0.56845T + 984.5679 \exp(\frac{w}{115.96277}))}{5610.5} \quad (3.8)$$

where w is the weight percentage content (%wt) of KOH in water.

Other authors [65, 54, 64] has extended the previous model considering also the effect of pressure in 3.1:

$$V_c = OCV + ((r_1 + d_1) + r_2 \cdot T + d_2 \cdot p) \cdot i + s \cdot \log\left(\left(t_1 + \frac{t_2}{T} + \frac{t_3}{T^2}\right) \cdot i + 1\right) \quad (3.9)$$

The present model proposes a new equation for the modeling of alkaline electrolyzers taking into account the effect of temperature, pressure, electrolyte concentration

and distance between electrodes. The effect of electrolyte concentration C and distance between electrodes d is evaluated according to [17]. Introducing five new coefficients to the equation 3.9:

$$V_c = OCV + ((r_1 + d_1 + p_1 + q_1) + r_2 \cdot T + d_2 \cdot p + q_2 \cdot d + p_2 \cdot C + p_3 \cdot C^2) \cdot i + s \cdot \log\left(t_1 + \frac{t_2}{T} + \frac{t_3}{T^2}\right) \cdot i + 1 \quad (3.10)$$

It is important to take into account the effect of the concentration of the electrolyte, on the electrolyzer performance. Aqueous potassium hydroxide (KOH) is used as a primary electrolyte for alkaline electrolyzers, but also for alkaline fuel cells (AFCs) and alkaline batteries. A diluted electrolyte solution could make the ionic and electronic transport not sufficiently fast, resulting in an increase of the ohmic overvoltage, in particular an increase of the resistive contribution of R_{ions} . However also a too highly concentrated solution (generally over 40%) could lead to fast corrosion problems in materials in contact with the electrolyte, and a decrease in the specific conductivity [70]. The specific conductivity is defined as the capacity to transfer ions and electric species in S/cm^2 .

A trend with a central peak, could be observed considering the effect of the distance between anode and cathode. This gap is really important because it represents the space that OH^- ions need to travel to reach the anode. The effect will be observed in the variation of the ohmic overvoltage in the alkaline electrolysis cell. Decreasing the width of the chamber, will correspond to an increase of the overall conductivity, due to the shorter path ions need to travel, between the two electrodes. On the other hand, when considering very high current densities, reducing the spacing too much will results in a total reduction of the conductivity and correspondingly an increase of η_{ohm} and the energy needed for the electrolysis process [38]. In particular conditions, as the use of porous electrolytes which enhances the bubble detachment, the optimal distance cannot be reached and is convenient to reduce the electrode-electrode path as much as possible, to reduce the required potential for the electrolysis. At increasing electric currents, the decreasing effect of V_c is more conspicuous.

Resuming the present model is able to describe the polarization behaviour according to the variation of four operating conditions. This effect could be designed, merging different semi-empirical models proposed in literature; in particular the effect of temperature from [11], the effect of pressure according to [65], and finally the effect of electrolyte concentration and distance of electrodes from [17].

3.1.2 Faraday efficiency

The Faraday efficiency (η_F), is the most useful efficiency for electrolyzer, because it specifies the real amount of hydrogen produced versus the theoretical value.

η_F is mainly dependent on parasitic current losses, which increases at decreasing current density, because of an increasing share of electrolyte [71]. Also temperature affects the Faraday efficiency lowering the resistance and increasing the parasitic current losses, for increasing temperature. For modeling the empirical expression is assumed as function of current density at a given temperature, proposed by [11]:

$$\eta_F = \frac{i^2}{f_1 + i^2} f_2 \quad (3.11)$$

In order to account for the effect of temperature as a variable, [65] extended the two parameters (f_1 and f_2) as:

$$f_1 = f_{11} + f_{22} \cdot T \quad (3.12)$$

$$f_2 = f_{21} + f_{22} \cdot T \quad (3.13)$$

The effect of pressure on the Faraday efficiency shows very slight influences, so that it is not accounted for in this model [65].

3.1.3 Mass balance

The hydrogen production rate defined as in equation 2.72 for the ideal case, could be extended in molar terms as:

$$\dot{n}_{H_2} = \eta_F \frac{n_c I}{zF} \quad (3.14)$$

or in other words is directly proportional to the transfer rate of electrons at the electrodes, which in turn is equivalent to the electrical current in the external circuit. The model accounts for an electrolyzer composed of n_c cells connected in series.

Finally the water consumption could be calculated simply from stoichiometry (2.1), as the oxygen production rate.

$$\dot{n}_{H_2O} = \dot{n}_{H_2} = 2\dot{n}_{O_2} \quad (3.15)$$

Differently from what described in [64], the mole flow rate at the cathode is defined as:

$$\dot{n}_{H_2,cat} = \dot{n}_{H_2} - \dot{n}_{H_2,an} \quad (3.16)$$

in which $\dot{n}_{H_2,an}$ is the amount of hydrogen diffused into the anode side, accounted by HTO

$$\dot{n}_{H_2,an} = HTO \cdot \dot{n}_{O_2} \quad (3.17)$$

Once calculated the mole flow rate at anode and cathode, the mass flow rate at the cathode is calculated imposing the mass balance equation:

$$\dot{n}_{in} \cdot MW_{in} = \dot{n}_{an} \cdot MW_{an} + \dot{n}_{cat} \cdot MW_{cat} \quad (3.18)$$

where \dot{n}_{in} , \dot{n}_{an} , \dot{n}_{cat} represent the mole flow rates of inlet, anode and cathode streams respectively, and MW their mean molar weight.

The inlet solution is assumed to split half in the anode and half in the cathode. The anode stream is imposed to be composed by oxygen (\dot{n}_{O_2}), hydrogen diffused into the anode ($\dot{n}_{H_2,an}$), and half of the inlet solution deprived by the consumed water (\dot{n}_{H_2O}). The molar fraction of oxygen in the cathode stream is considered negligible. The presence of hydrogen and oxygen in the inlet stream is imposed to split totally to the cathode and anode, respectively; the model presents a unique inlet stream, but the mass balance take into account the separated path of cathode and anode recirculation in a real plant.

3.1.4 Energy balance

The total energy demand is represented by the enthalpy of the reaction 2.10. If all the energy is provided by electricity, the cell voltage is corresponding to the thermoneutral voltage V_{tn} (equation 2.31). In case the cell voltage is higher than the thermoneutral voltage, a cooling device would be needed for removing the excess heat; in case the voltage provided is lower than the V_{tn} , external heat should be supplied to make the reaction favourable. This excess heat could be calculated as the difference between the generated heat and the heat losses.

$$Q_{excess} = Q_{gen} - Q_{loss} \quad (3.19)$$

where [64]:

$$Q_{gen} = n_c \cdot I(V_c - V_{tn}) \quad (3.20)$$

A positive excess heat will result in an increase of temperature of the electrolyte and of the oxygen and hydrogen streams; this heat must be removed to maintain a controlled temperature. The equation 3.19 could be used in steady state characterization of the system, accounting for no temperature variation inside the electrolytic cell.

The first law of thermodynamic is considered in order to make the stack be in energy balance. In particular, considering a fixed stack volume, the enthalpy variation between the inlet streams equals the mathematical sum of work imposed on the system and heat produced by the system (eq. 2.11).

3.1.5 System efficiency

The system efficiency account for the higher heating value of hydrogen, divided by the power input to the entire plant [72].

$$\eta_{system} = \frac{n_{H_2,prod} \cdot HHV_{H_2}}{W_{system}} \quad (3.21)$$

where W_{system} is the total power input to the system, including both stack power and BOP components.

3.2 Thermal model

Thermal models of alkaline electrolyzers are used in order to describe the temperature behaviour of the system. Different thermal models were proposed in literature. Ulleberg [11] proposed a model to predict the temperature variation under varying operating conditions. It is based on the estimation of the thermal balance through the lumped thermal capacitance model. The effects of the heat losses and cooling heat are subtracted from the generated heat due to chemical reactions. Then the temperature of the electrolyzer is evaluated considering a quasi steady-state thermal model, choosing time steps sufficiently small. A similar approach is proposed in [66]. The lumped thermal capacitance model is always used for the estimation of the electrolyzer temperature; however, the heat generation term is split into the contribution of power input dissipated as heat minus the contribution of the enthalpy of exiting streams and the enthalpy gained by inlet water stream. Another path for the operating temperature estimation is proposed in [67]. The electro-thermal behaviour is described by the contribution of four heat coefficient: one considering the heat brought in the system per unit of time, another accounting for the heat generated by electrochemical reaction inside the cell, another for the heat dissipation through the environment, and last the heat transferred by the heat exchanger. The model permits to estimate the warm-up time of the electrolyzer to operative condition. It becomes of particular importance in case of coupling of the system with intermittent renewable generators; that could lead to frequent shut down or plant partial load operations.

3.2.1 Lumped thermal capacitance method

The temperature estimation is carried out using the lumped thermal capacitance method [11]. Temperature is considered constant inside the electrolyzer. The heat balance in a control volume is defined as:

$$C_t \frac{dT}{dt} = \dot{Q}_{gen} - \dot{Q}_{loss} - \dot{Q}_{cool} \quad (3.22)$$

where \dot{Q}_{gen} , \dot{Q}_{loss} and \dot{Q}_{cool} are the generated, losses and cooling heat flow, respectively.

$$\dot{Q}_{gen} = n_c(V_c - V_{tn})I = n_c \cdot V_c \cdot I(1 - \eta_c) \quad (3.23)$$

$$\dot{Q}_{loss} = \frac{(T - T_a)}{R_t} \quad (3.24)$$

$$\dot{Q}_{cool} = C_{cw}(T_{cw,in} - T_{cw,out}) = UA_{hx} \cdot LMTD \quad (3.25)$$

and

$$LMTD = \frac{(T - T_{cw,in}) - (T - T_{cw,out})}{\ln[(T - T_{cw,in}) - (T - T_{cw,out})]} \quad (3.26)$$

R_t is the electrolyzer resistance and the UA-product represents the heat exchanger coefficient for cooling water. Both the variables, and the thermal capacitance (C_t) must be determined empirically before solving the system of equations.

The equation 3.22 could be turned into a quasi steady-state thermal model, assuming constant heat generation and heat transfer rates for a given time interval, and choosing time steps sufficiently small.

$$T = T_{ini} + \frac{\Delta t}{C_t}(\dot{Q}_{gen} - \dot{Q}_{loss} - \dot{Q}_{cool}) \quad (3.27)$$

The lumped thermal capacitance (C_t) is the overall thermal capacitance of the electrolyzer [73]. It is defined as the sum of thermal capacitance of every component:

$$C_t = \sum_j \rho_j \cdot V_j \cdot \dot{c}_j \quad (3.28)$$

where ρ_j , V_j and \dot{c}_j are the density, volume and specific heat, respectively, of each of the electrolyzer components j . Despite, estimation of the different components in the equation could be done, the evaluation of the thermal capacitance could be very complex. An approximated equation could be defined in order to employ the process in practical applications.

$$C_t = \frac{P_{heat}}{dT/dt} \quad (3.29)$$

The previous equation was evaluated after experimental estimation [66], and the term related to the enthalpic term of inlet/outlet streams is neglected.

The UA-product account for both conduction and convection phenomena:

$$UA_{hx} = h_{cond} + h_{conv}I \quad (3.30)$$

This relation could be explained physically by the fact that an increase of current, and so of bubble production, will increment the mixing of the electrolyte, enhancing the heat transfer.

3.3 Gas purity model

Generally, the purity of the produced gases of electrolysis is higher compared to the ones produced from fossil fuels. In the electrolysis process this purity is dependent on the current density. It is of particular importance in case of electrolysis from renewable energy sources. The contamination of produced gases is relevant at lower current densities, as could happen in case of intermittent generation from renewable sources as PV or wind power [54]. This phenomenon is induced because at low current densities, diffusion processes through diaphragms and sealing reduce the purity of the produced gases [68]. However this phenomenon is not affecting the hydrogen gas too much; the oxygen content in hydrogen (*OTH*) varies approximately between 0.1 – 0.5%, therefore no special considerations are necessary, because usually the explosion limit is far away [74, 44, 71]. In operation modeling this contribution could be neglected. The most critical parameter results the hydrogen in oxygen content (*HTO*), also due to the higher hydrogen production rate, in a molar ratio of 2 : 1. It is a parameter describing the impurities of hydrogen in the anode outlet. The diffusion of product gases through the separator is enhanced at low current densities; it is deleterious for the quality of gas and in terms of electrolysis efficiency, because hydrogen and oxygen can react together to form water [44]. A way to calculate its theoretical value, it is to use diffusion coefficients and solubility of gases [44]. From the moment that these parameters are of difficult estimation, an empirical model, proposed in [65], is adopted for the determination of the gas impurities.

$$\begin{aligned}
 HTO = & c_1 + c_2 \cdot T + c_3 \cdot T^2 + (c_4 + c_5 \cdot T + c_6 \cdot T^2) \exp\left(\frac{c_7 + c_8 \cdot T + c_9 \cdot T^2}{i}\right) \\
 & + e_1 + e_2 \cdot p + e_3 \cdot p^2 + (e_4 + e_5 \cdot p + e_6 \cdot p^2) \exp\left(\frac{e_7 + e_8 \cdot p + e_9 \cdot p^2}{i}\right) \quad (3.31)
 \end{aligned}$$

The equation 3.31 shows the dependence of the impurities in oxygen from the current density (i), the temperature and the pressure. In particular c_1 to c_9 constants represents the influence of the temperature, while e_1 to e_9 the affinity of pressure with *HTO*.

In order to evaluate experimentally the 18 coefficients, a fixed pressure experiment should be carried out to evaluate c_1 to c_9 . Then using the discovered constants, the e coefficients are evaluated at constant temperature conditions.

3.4 Parameters fitting

In order to obtain all the parameters of the model, a systematic procedure is followed, as described in [17]. The process consists of a non-linear regression of the

model on experimental data. The tool is implemented in Matlab. The methodology consists of the following steps:

- **Step 1** Determination of the "s" parameter applying the Matlab function `lsqcurvefit` on the basic polarization equation 3.1. The data used are at fixed T , p , C and d . Initial values of "t" and "r" are also calculated.
- **Step 2** Treat the obtained "s" value as constant. Polarization curve obtained at other 2 temperatures (T_2 and T_3) are used to obtain two different values of the parameter "r". These values are used in equation 3.2 to obtain the values of r_1 and r_2 . These obtained values will be used as guessing values in a second iteration.
- **Step 3** Having "s", " r_1 " and " r_2 ", it is possible to evaluate the parameter "t". In order to do so, the same experimental data at three different temperatures used before, are applied in `lsqcurvefit` to the polarization equation with three known parameters. As done for "r" the parameters " t_1 ", " t_2 " and " t_3 " are obtained from the values of "t" at different temperatures.
- **Step 4** Knowing the temperature parameters, the procedure is repeated to determine the pressure parameters "d". The non-linear regression is applied on I-V curve data corresponding to different pressures with the equation 3.9. Considering at least two pressure variations, it is possible to evaluate " d_1 " and " d_2 " from "d".
- **Step 5** The effect of the electrolyte concentration is considered using parameters "p". Using experimental data of cell voltage and current density, it is possible to obtain different values of "p" at different values of concentration (%wt); they are used to obtain " p_1 ", " p_2 " and " p_3 ", as done in previous steps. The parameter "p" is considered as zero at the starting concentration.
- **Step 6** Fixing the coefficients previously obtained, it is evaluated the effect of the electrodes distance with the coefficient "q". The parameter "q" is considered as zero at the initial distance.
- **Step 7** At the end, all the calculated parameters are used as starting guess values in the retrofitting procedure, from step 1.

A reasonable initial guess is needed in order to avoid the retrofitting to have imaginary solution. Steps 5 and 6 aren't used in the following model application.

After completing the procedure, all the parameters are determined with an acceptable accuracy. A similar procedure is used to determine the four parameters, for the description of the Faraday efficiency. Starting with the determination of the

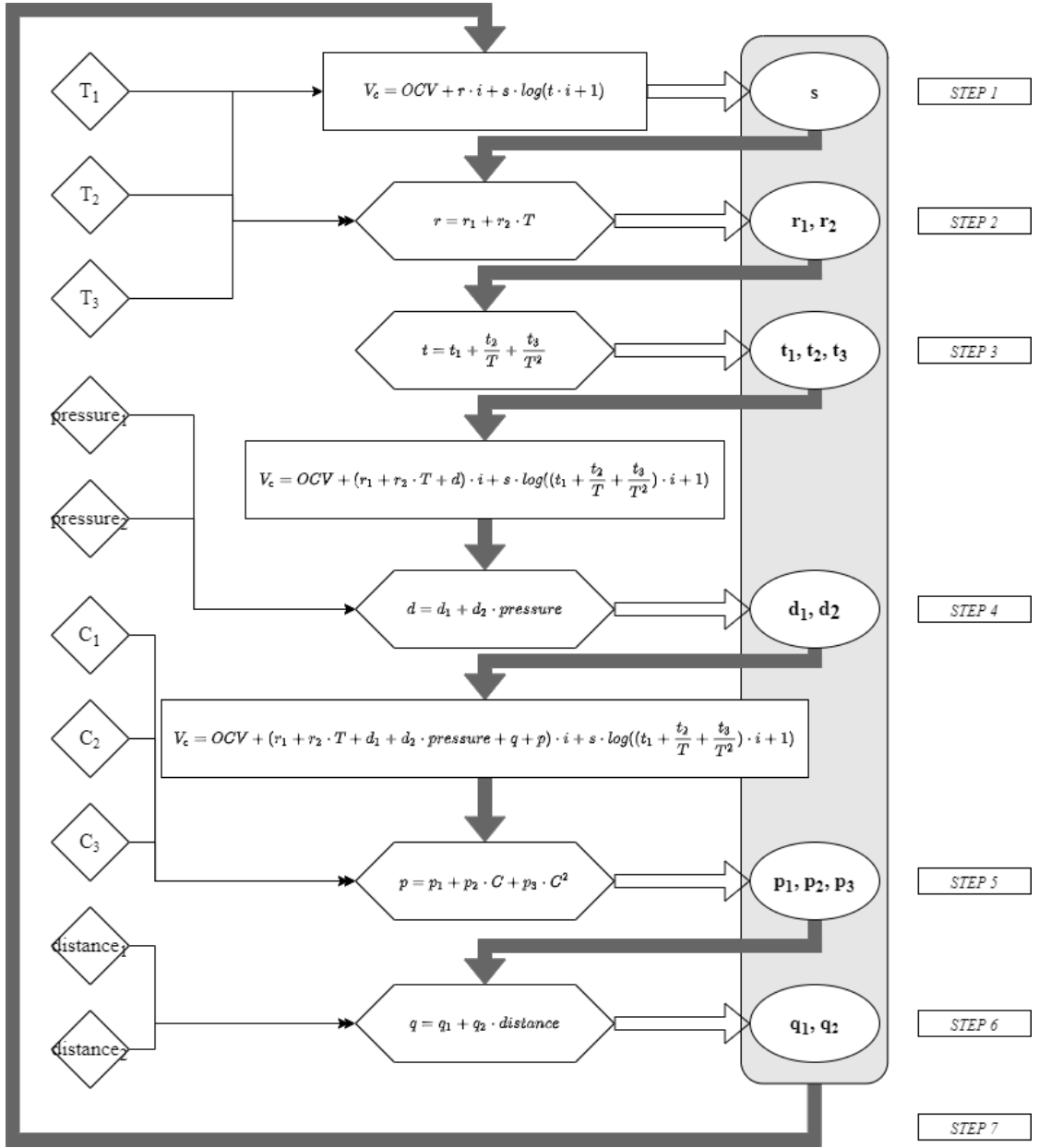


Figure 3.1: Procedure for the determination of the cell voltage parameters. The diamonds on the left express the experimental data evaluated at those conditions.

two temperature dependent coefficients " f_1 " and " f_2 " with non-linear regression on experimental data. Finally the four coefficients are determined as in equation 3.12.

The hydrogen in oxygen content equation is governed by 18 parameters, half for the description of the temperature effect and half for the pressure effect. The

regression procedure is done, firstly considering only the temperature effect, and rearranging the coefficients in groups of three; every coefficient describe a quadratic relation with temperature as unknown variable. The definition of these parameters is done using the non-linear regression tool in Matlab, as described previously. The evaluation is done at three different values of temperature in order to get the coefficients from "c₁" to "c₉". They are then used as initial values in the next iteration step. The effect of pressure is accounted for, considering the temperature coefficients as constants. The same process for temperature is repeated for pressure.

It is important to define the working range of the model, in order to not income in convergence problems. The model must be calibrated with experimental data with the process described above. The minimum and maximum values for operating current, stack temperature and pressure are defined at the moment of experimental testing. Ranges for the model used in this work are $i = 80 - 500 \text{ mA/cm}^2$, $T = 55 - 85 \text{ }^\circ\text{C}$ and $P = 5 - 9 \text{ bar}$.

3.5 Aspen modeling

To describe the electrolytic system in Aspen Plus, the first step is to determine an appropriated set of properties. In the presented case the ENRTL-RK¹ (electrolyte nonrandom two liquid) model with Redlich-Kwong equation of state is used; as suggested in [64]. The properties with the compounds are exported in ACM. The electrolysis stack is modeled considering the governing equations and the imported properties. A simulation is run to verify the operation of the stack model. Finally, the model is exported into Aspen Plus, where it is assessed in the complete electrolyzer system.

3.5.1 Electrolytic stack model

The model of the alkaline stack for water electrolysis is implemented in Aspen Custom Modeler. First of all the components used in the simulation are uploaded from the Aspen property file created before. The chemical compounds used are grouped under the component "Default". The "AELSTACK" model is created. The model is initialized defining the variables and parameters to be used in the equations. The set of equation used are the electrochemical equations, mass balance and energy balance equations antecedently described. Another set of equations are added in order to define the composition of the outlet streams (cathode, anode and solution outlet). Follows the definition of ports which are used to define which process variable information is transferred between models and streams; they permit

¹For a detailed explanation of the model check [75]

the model to relate with the system. Three material ports are created to account for: the inlet solution port ("Feed"); the outlet cathode and anode ports, "CatOut" and "AnOut" respectively. An additional fictitious port "Out" is defined to account for the energy calculation; a negligible water mass flow is imposed in this port in order to perform enthalpy and Gibbs free energy calculation for the water splitting reaction. A work inlet port "EleIn" is used for the definition of the employed power in the process, and a heat outlet port "HeatOut" is defined for account the excess heat produced in the stack; the heat port accept both positive and negative values, in order to characterize the operations over and under the thermo-neutral voltage. Ports are created only after the "AELSTACK" model is implemented and working properly. Streams are special types of model in ACM; they can be connected in input or in output to blocks and can contain a set of equations. The streams used for the model are the pre-defined "Connections", able to characterize enthalpy, mole flow, temperature and pressure. At the end, a steady state simulation is run, in order to evaluate the convergence of the proposed model. The model is ready to be exported in Aspen Plus as a block, and to operate as part of the final system.

3.5.2 System model

The electrolyzer model is able to characterize the cell's behaviour from the inlet solution to the formation of the products. In order to characterize the entire electrolyzer, the electrolysis stack is connected to auxiliary components in Aspen Plus. The model consists in an electrolyzer stack with two outlet stream. A separation unit is considered downstream the electrolyzer for the separation of the solution from the valuable products, considering adiabatic conditions; in order to increase the purity of hydrogen and oxygen a further separation step is employed, tearing down the temperature to ambient values. The liquid streams coming out from the first step separators are recirculated to the inlet, by means of a pump and a cooler to restore initial temperature and pressure. A mixer is used in order to blend the recirculation loops with the inlet water stream accounting for the water consumed in the process. The recirculation solution is split before the mixer and the same stream composition and conditions are imposed at the interruption; two "design-spec" blocks, one for the anode and one for the cathode side, impose the same mass flow of K^+ ions between the exit of the cooler and the inlet of the mixer. The mass flow of the inlet water stream is set by means of "design-spec" block; the inlet is calculated in order to balance the electrolysis water consumption, considering the mass flows exiting the system. The base-case flowsheet in Aspen Plus is showed in fig.3.2.

Chapter 4

Results and Discussion

In order to simplify the process, the following assumptions are made:

- The process works at steady state conditions
- Deionised water is provided in inlet to the system
- Hydrogen and oxygen output are at 1 *bar* and 25°C
- The excess heat is removed maintaining the electrolyzer temperature constant
- The heat losses are evaluated with the respect to ambient temperature

4.1 Coefficient estimation

On the basis of the experimental data, the coefficients for the model are evaluated applying the Matlab regression procedure described in chapter 3. Results are showed in the table 4.1; they are used for the initialization of the model. The procedure revealed to be sensitive to the initial values used in the regression process; wrong predictions made the tool to converge to complex numbers. To solve this problem, the coefficients obtained after the first iteration are used as initial guesses in the following step. The units of measurement of the coefficients refer to an evaluation of the current density in A/m^2 , the temperature in °C and the pressure in *bar*. It is possible to use different units of measurement for the coefficient estimation, if remaining coherent with the model parameters.

Table 4.1: Coefficient evaluation from experimental data.

| Model | Coefficient | Value | Unit |
|--------------------|-------------|-------------------|-------------------------|
| Polarization curve | r_1 | 7.4358e-5 | Ωm^2 |
| | r_2 | -1.918e-7 | $\Omega m^2 / ^\circ C$ |
| | d_1 | -1.0688e-5 | Ωm^2 |
| | d_2 | 1.425e-6 | $\Omega m^2 / bar$ |
| | s | 0.2264 | V |
| | t_1 | 0.4948 | m^2 / A |
| | t_2 | -71.4403 | $m^2 / (A^\circ C)$ |
| | t_3 | 2905.3 | $m^2 / (A^\circ C^2)$ |
| Faraday efficiency | f_{11} | 4.7865e5 | A^2 / m^4 |
| | f_{12} | -2952.5 | A^2 / m^4 |
| | f_{21} | 1.0396 | - |
| | f_{22} | -0.0011 | $1 / ^\circ C$ |
| Gas purity | c_1 | -0.0625 | - |
| | c_2 | 0.0024 | $1 / ^\circ C$ |
| | c_3 | -1.7852e-5 | $1 / ^\circ C^2$ |
| | c_4 | 0.0951 | - |
| | c_5 | -0.0033 | $1 / ^\circ C$ |
| | c_6 | 2.4506e-5 | $1 / ^\circ C^2$ |
| | c_7 | -3422.6 | A / m^2 |
| | c_8 | 82.2711 | $A / (m^2 ^\circ C)$ |
| | c_9 | -0.7175 | $A / (m^2 ^\circ C^2)$ |
| | e_1 | 237.5627 | - |
| | e_2 | -80.6093 | $1 / bar$ |
| | e_3 | 6.2747 | $1 / bar^2$ |
| | e_4 | -237.5707 | - |
| | e_5 | 80.6116 | $1 / bar$ |
| | e_6 | -6.2749 | $1 / bar^2$ |
| | e_7 | -0.0348 | A / m^2 |
| e_8 | -0.013 | $A / (m^2 bar)$ | |
| e_9 | 0.0018 | $A / (m^2 bar^2)$ | |

4.2 Matlab simulations

The obtained parameters, from the previous step, are used to initialize the model in Matlab. In particular, the following figures depict the retrofitting curves with the experimental data. The root mean square error of each variable x is being

evaluated according to the formula:

$$RMS_{error} = \sqrt{\frac{\sum (x_{th} - x_{exp})^2}{N - 1}} \quad (4.1)$$

where x_{th} is the theoretical values from data, and x_{exp} is the value obtained from the fit, N is the number of points evaluated.

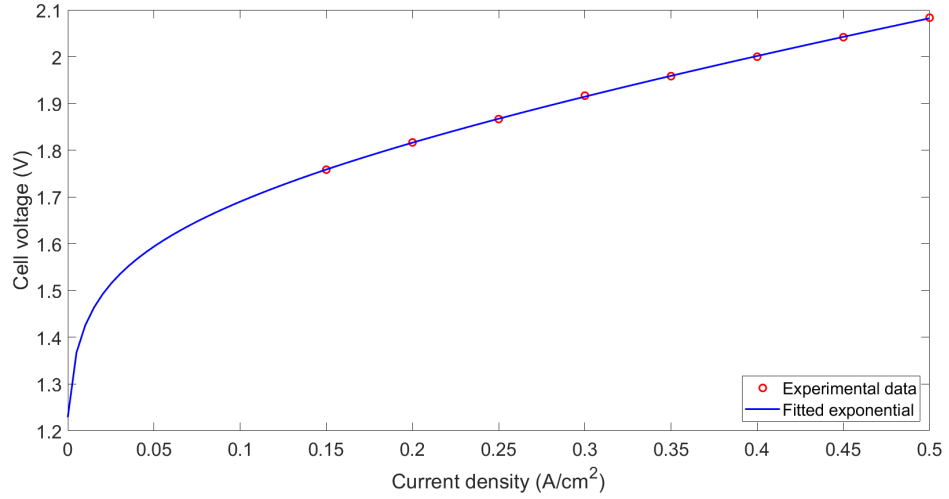


Figure 4.1: Fitted Polarization behaviour modeled (curve) and experimental data (dots).

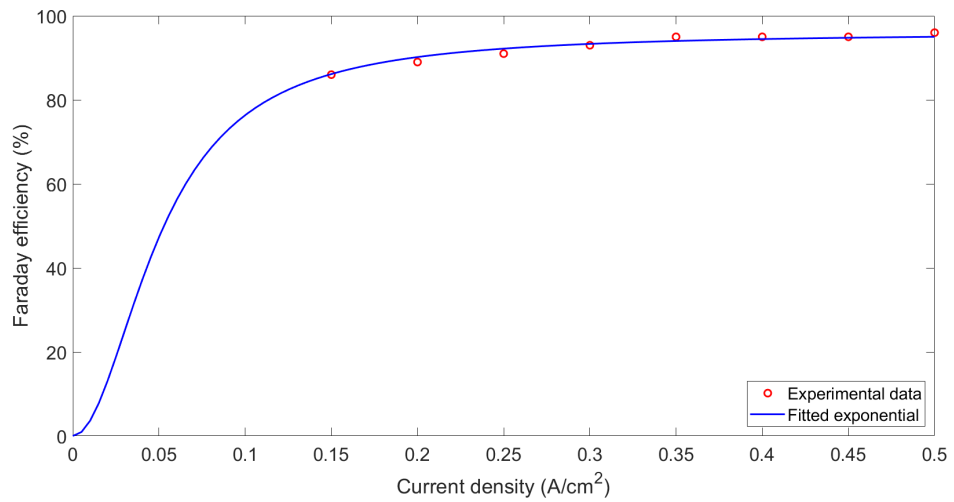


Figure 4.2: Fitted Faraday efficiency (curve) and experimental data (dots).

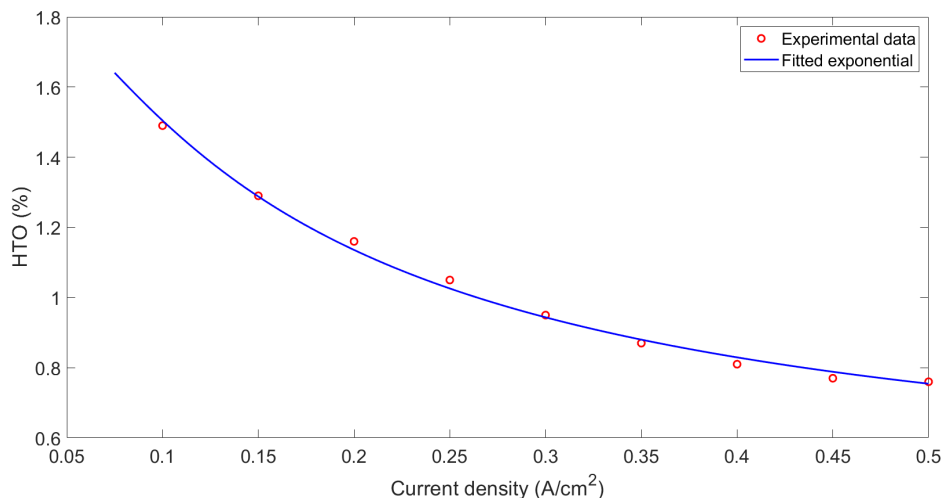


Figure 4.3: Fitted gas purity (curve) and experimental data (dots).

All the curves are obtained considering an operative $T = 75\text{ }^{\circ}\text{C}$ and $p = 7\text{ bar}$. The experimental data are obtained from [65]. The actual parameters depict a step increase of the cell voltage in the first part of the graph (4.1). In order to describe the accuracy of the predicted curve, the RMS error is calculated for the cell voltage. It shows an average value of 7.6 mV . The model curve (solid line) seems to predict the experimental points well. However, more experimental points can be useful in predicting the low current density behaviour. All the curves follow the experimental trend faithfully. The Faraday efficiency shows an average RMS error of 1.2%, while the HTO only gives a value of 0.02%. The HTO increases as the current density decreases. It is important to avoid operations at low current densities in order to avoid the creation of explosive mixtures.

4.3 Aspen Plus simulation

After the creation of the electrolysis cell model in ACM, and the complete system setup in Aspen Plus, the simulation is run and results obtained. The base case Aspen solution, $T = 75\text{ }^{\circ}\text{C}$ and $p = 7\text{ bar}$, is shown in figure 4.4. The table 4.2 shows the composition of the principal streams. Streams MIXINA and MIX-IN-A are imposed to be equal, as well as MIXINC matches MIX-IN-C; for this reason neither of them are presented in the table. The system as described in 4.4 is working with a power of 10 kW , corresponding to a current density of $i = 0.42\text{ A/cm}^2$. The hydrogen production is 0.18 kg/h (without accounting water content), corresponding to a volume flow of $2\text{ Nm}^3/\text{h}$ of H_2 at $25\text{ }^{\circ}\text{C}$ and 1 bar . The energy is balanced in the stack, considering the cooling of an excess 2289.8 W of heat.

Table 4.2: Material flow composition at base case (T=75°C and p=7 bar).

| Stream | T (°C) | P (bar) | Mass flow (kg/h) | Molar fraction | | | | |
|----------|-----------|------------|---------------------|----------------|--------|--------|-------|-------|
| | | | | K^+ | OH^- | H_2O | O_2 | H_2 |
| H2O_IN | 75 | 7 | 1.725 | 0 | 0 | 1 | 0 | 0 |
| MIXINA | 75 | 7 | 60.260 | 0.141 | 0.141 | 0.716 | 0.003 | 2e-5 |
| MIXINC | 75 | 7 | 89.524 | 0.090 | 0.090 | 0.818 | 0 | 0.003 |
| STACK_IN | 76.17 | 7 | 151.508 | 0.108 | 0.108 | 0.781 | 0.001 | 0.002 |
| CATOUT | 79.42 | 7 | 89.787 | 0.088 | 0.088 | 0.802 | 0 | 0.022 |
| H2 | 79.37 | 6.7 | 0.263 | 0 | 0 | 0.049 | 0 | 0.951 |
| H2_OUT | 25 | 6.4 | 0.188 | 0 | 0 | 0.005 | 0 | 0.995 |
| ANOUT | 79.38 | 7 | 61.721 | 0.138 | 0.138 | 0.705 | 0.018 | 1e-4 |
| O2 | 79.36 | 6.7 | 1.461 | 0 | 0 | 0.035 | 0.957 | 0.008 |
| O2_OUT | 25 | 6.4 | 1.436 | 0 | 0 | 0.005 | 0.987 | 0.008 |
| PURG_CAT | 25 | 6.4 | 0.075 | 0 | 0 | 0.999 | 0 | 9e-5 |
| PURG_AN | 25 | 6.4 | 0.025 | 0 | 0 | 0.999 | 1e-4 | 7e-7 |
| R_CAT | 79.37 | 6.7 | 89.524 | 0.090 | 0.090 | 0.818 | 0 | 0.003 |
| R_AN | 79.36 | 6.7 | 60.260 | 0.141 | 0.141 | 0.716 | 0.003 | 2e-5 |

4.3.1 Study on explosive limits

When the recirculation loop is inserted, a part of oxygen and hydrogen dissolved in the water solution recirculates back to the inlet of the stack. If the inlet of the stack is unique, it is not possible to separate the incoming oxygen and hydrogen to the anode and cathode outlet, respectively. The effect will be the presence of oxygen in the cathode stream and an amount of hydrogen in the anodic side, additionally to the HTO content. A study is made in order to evaluate the values of the impurities and if they can be considered hazardous at particular operative conditions. As explained in the paragraph 2.4.3 the lower and upper explosion limits are of 3.8 mol% and 95.4 mol% for H_2/O_2 -gas mixtures at atmospheric pressure and 80°C [45]. The results show that under normal condition no problems arise for both anode and cathode side. The main factor affecting the impurities seems to be the current density i and correspondingly the electric power W_{el} .

4.4 Validation of Matlab model

The following graphs show the variation of the main variables defined by the model, at different current densities. Each figure shows the Matlab results on the left side and the Aspen plus results on the right plot. The main difference between the two software, consists in the calculation method of the open circuit voltage and

the thermo-neutral voltage; Aspen plus directly calculates those values from the definition (OCV in 2.20 and V_{tn} in 2.31) using Gibbs free energy and enthalpy values from its database, instead in Matlab, a model (subsection 3.1.1) was defined for OCV dependence from temperature and pressure.

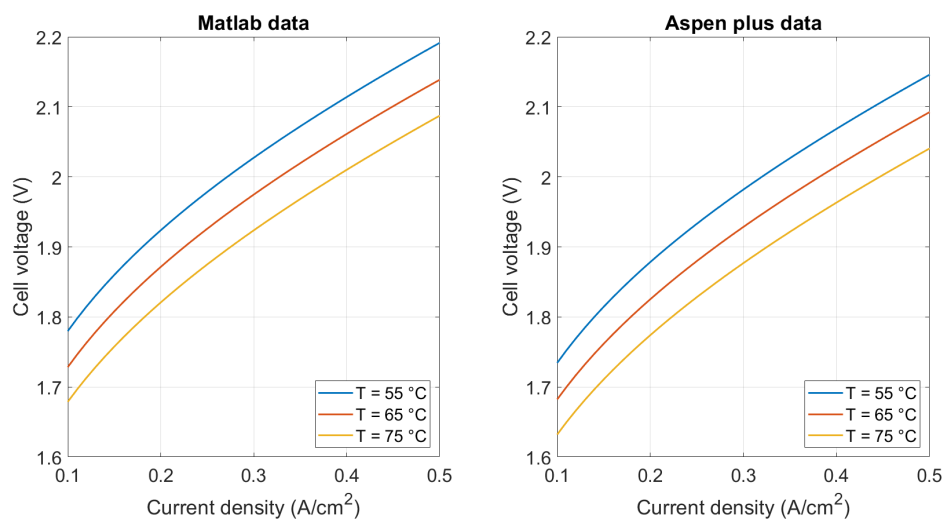


Figure 4.5: Matlab vs Aspen plus comparison of operative cell voltage at different temperatures.

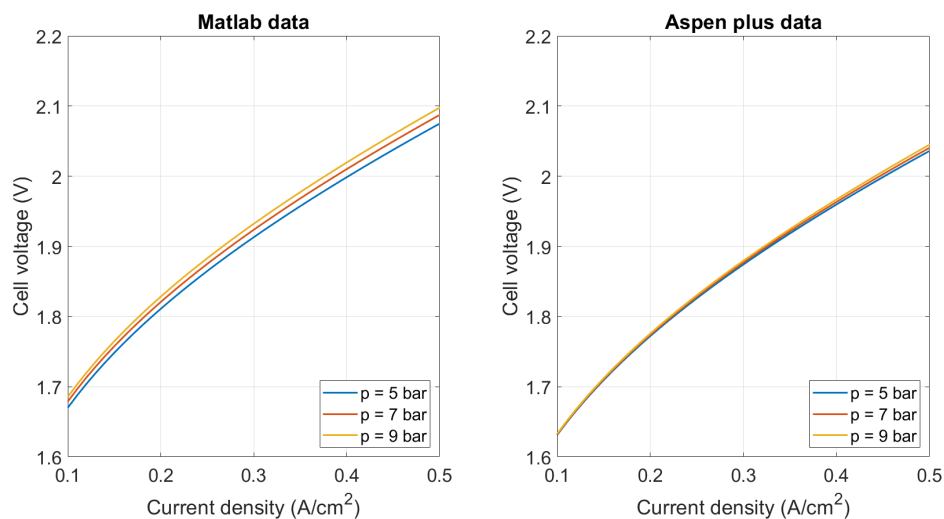


Figure 4.6: Matlab vs Aspen plus comparison of operative cell voltage at different pressures.

A slight difference could be noted between the two plots in figure 4.5. The

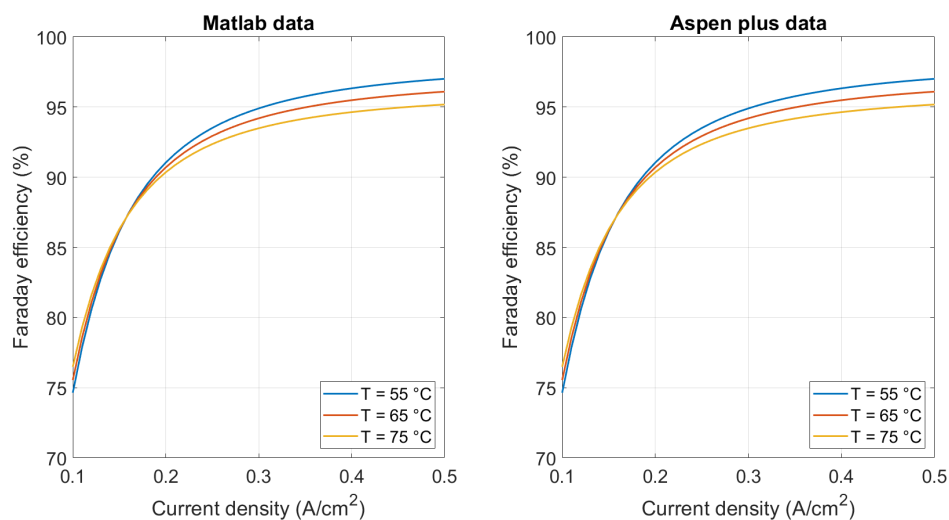


Figure 4.7: Matlab vs Aspen plus comparison of Faraday efficiency at different temperatures.

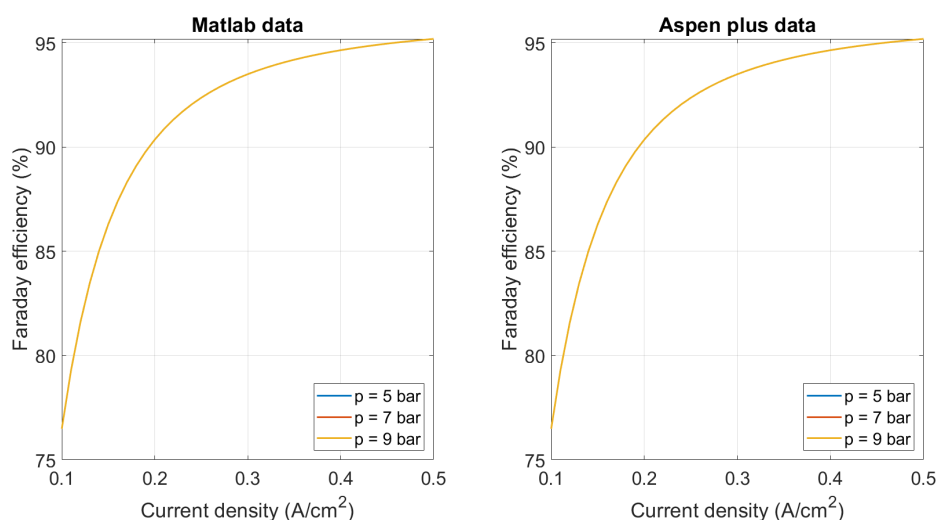


Figure 4.8: Matlab vs Aspen plus comparison of Faraday efficiency at different pressures.

different OCV calculation caused the Matlab model to overestimate the cell voltage through out all the current density range of about $+0.5 V$. A different event could be noted in figure 4.7. The effect of pressure seems to be more relevant in the Matlab plot. The phenomenon could be explained with the different OCV calculation. The effect of pressure in the OCV formula used in Matlab seems to be more effective than it should be.

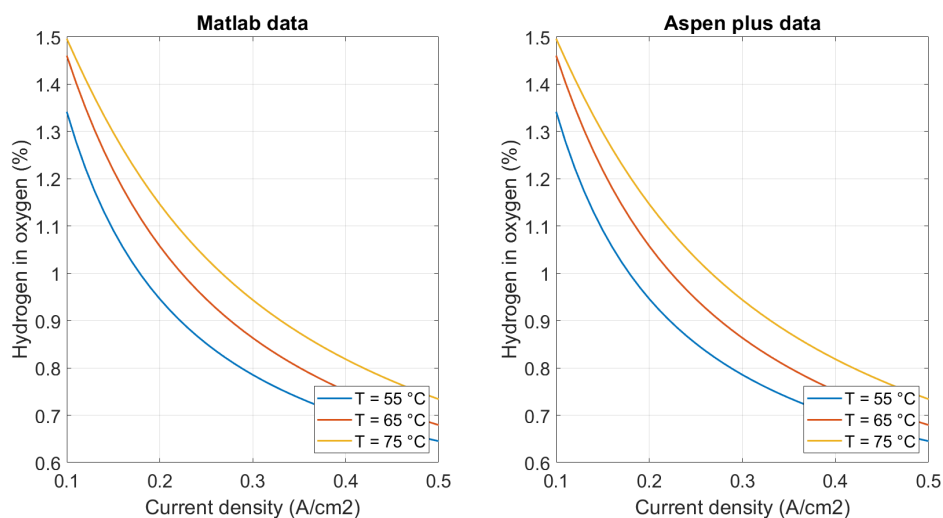


Figure 4.9: Matlab vs Aspen plus comparison of hydrogen in oxygen content at different temperatures.

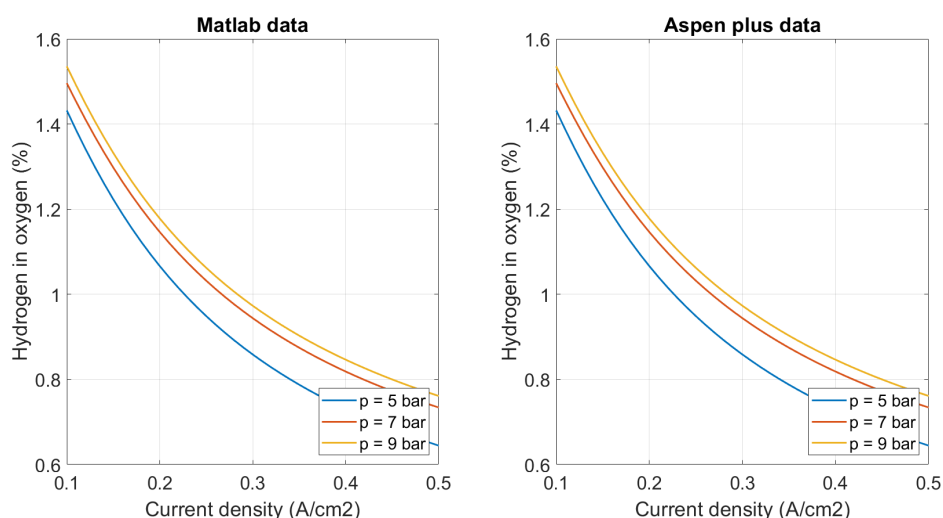


Figure 4.10: Matlab vs Aspen plus comparison of hydrogen in oxygen content at different pressures.

No appreciable differences could be noted in the graphs (4.7, 4.8, 4.9, 4.10) representing the Faraday efficiency variation and hydrogen in oxygen content variation with the current density. As can be noted, the Faraday efficiency curve shows same values at different pressures; it is modeled taking into account a negligible effect of pressure. The pressure affects the *HTO* negatively; it acts increasing the solubility of hydrogen in the solution, increasing the percentage of

molecules able to cross the diaphragm. The temperature is responsible for causing the same effect.

4.5 Comparison with commercial systems

In the table below (4.3) a comparison of the main characteristics of the modeled electrolyzer is presented, with two commercial alkaline electrolyzer from Cummins and Nel hydrogen. The experimental data used for the setup of the model are from [65]; they are collected from experimental tests bench developed by Centro Nacional del Hidrogeno (CNH2) on a 15 kW alkaline electrolyzer.

Table 4.3: Comparison table of the main electrolyzer model characteristic, with commercial datasheet by Cummins [76] and Nel hydrogen [77]. The data from the model are evaluated at 80 °C and 7 bar.

| Specifications | Model | Cummins | Nel |
|--|-----------------------------|--|-----------------------------|
| Net Production Rate | 2.3 Nm ³ /h | 10 Nm ³ /h | 150 Nm ³ /h |
| Production Capacity | 20-100% | 40-100% | 15-100% |
| Dynamic Range | of flow range | of flow range | of flow range |
| Power Consumption at Stack level | 4.7-5.2 kWh/Nm ³ | 4.9-5.4 kWh/Nm ³ | 3.8-4.4 kWh/Nm ³ |
| Purity – with optional purification | 99.5% | 99.998% | 99.99-99.999% |
| O ₂ -Content in H ₂ | Negligible | <2 ppm v | <2 ppm v |
| H ₂ O-Content in H ₂ | 5000 ppm v | - | <2 ppm v |
| Electrolyte Composition | 30% KOH aqueous solution | - | 25% KOH aqueous solution |
| Operative pressure | 3-9 bar | 10 bar | 1 bar |
| Feed Water Consumption | 0.9 l/Nm ³ | 1.2-2 l/Nm ³ of potable water | 0.9 l/Nm ³ |

The actual model is able to reproduce characteristics similar to commercial electrolyzers. The presence of water molecules in H_2 represents the only strong difference. The commercial technologies use high pressure dryers to eliminate the excess water, making the hydrogen produced suited for fuel cell applications. In the current model, the two separation steps are only able to separate the liquid solution from the gas. The employment of a pressure swing absorption stage should be accounted to get lower H_2O values in the outlet hydrogen stream. However, the present study does not address the modeling of this system. The net production

rate for the present model is calculated at $i = 0.5 \text{ A/cm}^2$; the specific power consumption range is calculated at $T = 80^\circ\text{C}$ and $p = 7 \text{ bar}$ with current density variation from 0.1 to 0.5 A/cm^2 . The value results higher with the respect to the Nel's electrolyzer, due to the smaller size of the investigated system; while it is analogous to Cummins' values, due to the similarity in size. The feed water consumption is evaluated from the actual consumption of the system modeled in Aspen Plus; considering the water inlet divided by the hydrogen net production at base-case conditions. The actual model can be used to analyze commercial alkaline electrolyzers, predicting accurately the main features. In particular, the initial retrofitting procedure is able to calibrate the model on different electrolyzers.

4.6 Parametric study

From the following figures, it is possible to observe the comparison between the results from the current model (on the left) and the results from [54]. Both models are calibrated on the same experimental data-sets.

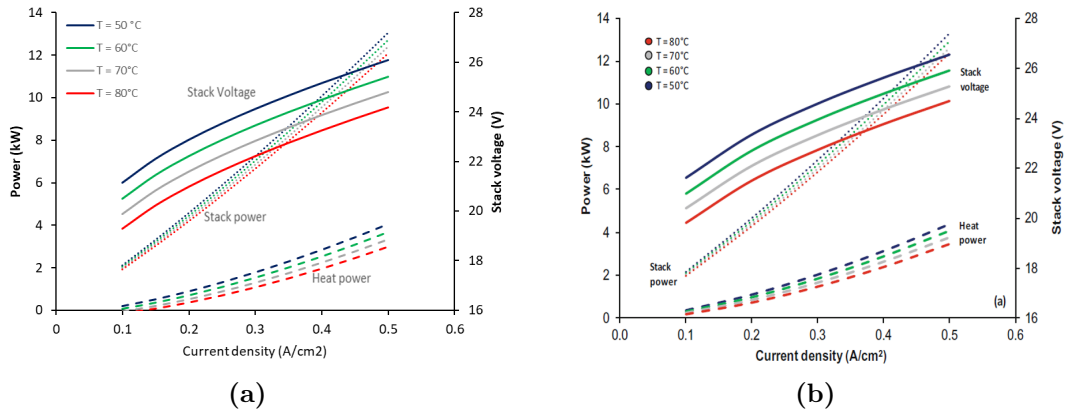


Figure 4.11: Polarization behaviour (solid curves), electric power inlet (dotted curves) and excess heat production (dashed curves), evaluated at different temperatures ($p = 7 \text{ bar}$): (a) data from current model; (b) data from [54].

The model describes an anti-proportional dependence between the temperature and the voltage of the cell. In particular, the stack voltage decreases passing from a temperature of 50°C to a temperature of 80°C . The difference seems proportional at every current density. Consequently, increasing the temperature decreases also the electrical power needed, at constant current density; maintaining the hydrogen production almost constant. The heat power decreases with the temperature as a consequence of the reduction of the stack power. Increasing the temperature has a

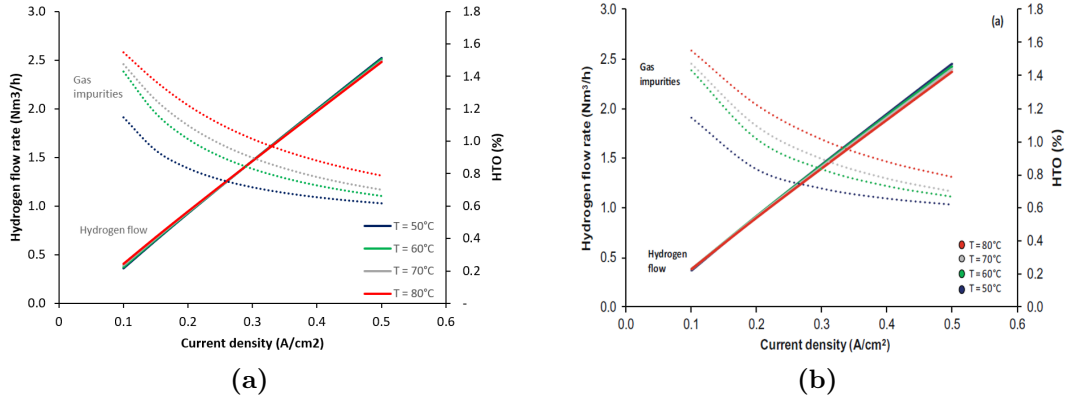


Figure 4.12: Hydrogen flow rate (solid curves) and hydrogen crossover in the anode (dotted curves), evaluated at different temperatures ($p = 7 \text{ bar}$): (a) data from current model; (b) data from [54].

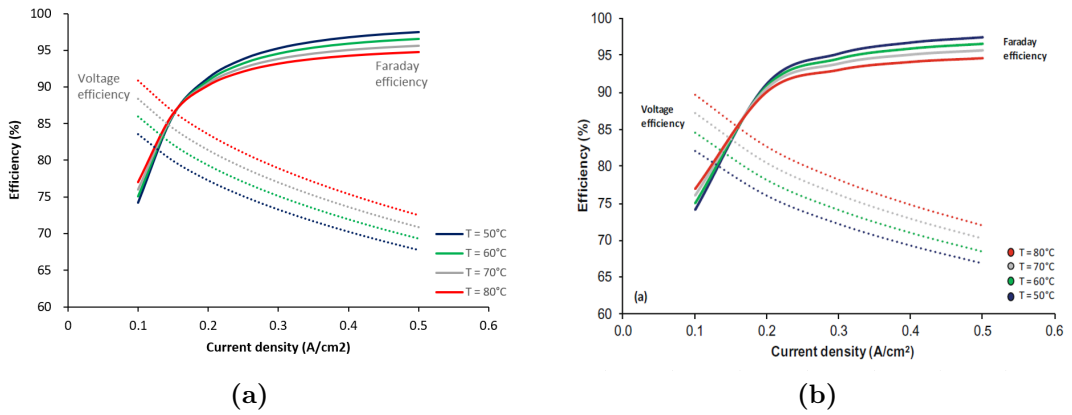


Figure 4.13: Faraday efficiency (solid curves) and voltage efficiency (dotted curves), evaluated at different temperatures ($p = 7 \text{ bar}$): (a) data from current model; (b) data from [54].

negative effect of reducing the Faraday efficiency for current density higher than 0.2 A/cm^2 , and of increasing the hydrogen leakage into the anode. The consequence is that the hydrogen production is slightly reduced by increasing the temperature (see fig.4.12).

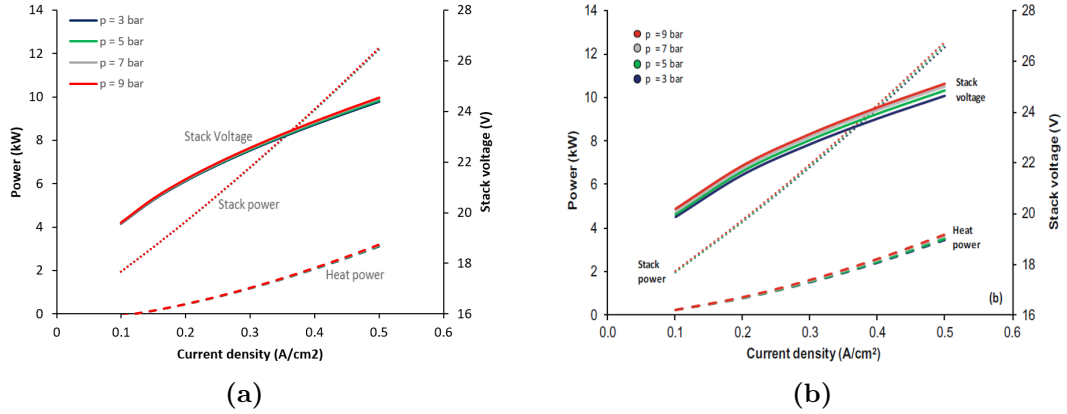


Figure 4.14: Polarization behaviour (solid curves), electric power inlet (dotted curves) and excess heat production (dashed curves), evaluated at different pressures ($T = 75^\circ\text{C}$): (a) data from current model; (b) data from [54].

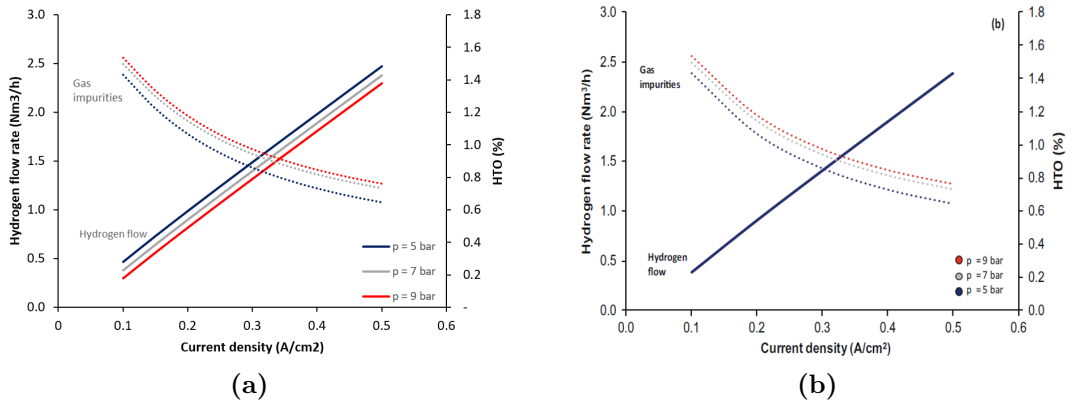


Figure 4.15: Hydrogen flow rate (solid curves) and hydrogen crossover in the anode (dotted curves), evaluated at different pressures ($T = 75^\circ\text{C}$): (a) data from current model; (b) data from [54].

The effect of pressure has a limited influence on the operative parameters. As can be seen from figure 4.13 the stack voltage increases with increasing pressure. This difference is more pronounced at higher current densities. The outcome is an higher stack power needed at constant current density. The pressure also influences negatively the hydrogen impurities in the oxygen stream. The hydrogen flow is affected by the pressure; an increase of pressure reduces the H_2 production.

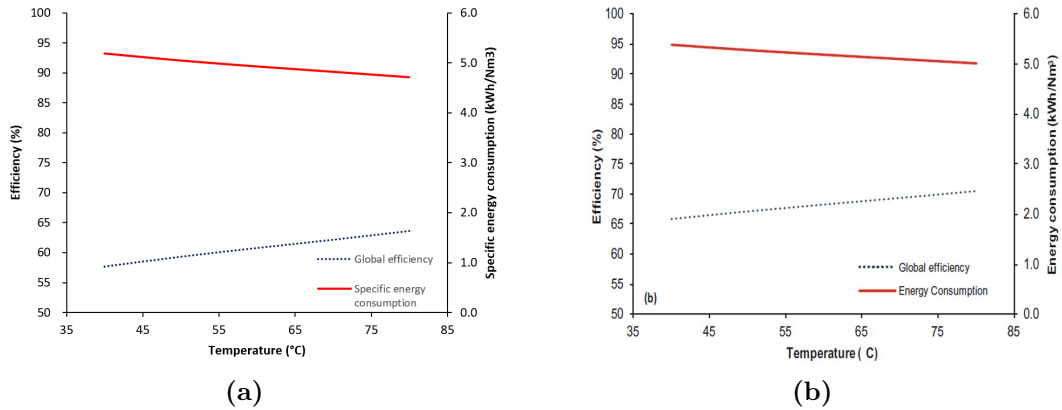


Figure 4.16: Specific energy consumption of the stack (solid curve) and global system efficiency (dotted curve), evaluated at $p = 7 \text{ bar}$: (a) data from current model; (b) data from [54].

The overall effect of temperature on the system is positive, considering the global efficiency (fig.4.16). Increasing the temperature from $40 \text{ }^{\circ}\text{C}$ to $80 \text{ }^{\circ}\text{C}$ increases the global efficiency from 58% to 64%. The specific energy consumption of the alkaline electrolyzer can be reduced by increasing the temperature; this is possible because the reduction of the electric power needed to drive the process is larger than the reduction of the hydrogen production, at a rated current density.

Chapter 5

Conclusion

The aim of this thesis was to create a model for an alkaline electrolyzer. In particular the model was implemented in Aspen plus, with the objective of evaluating the performances of a complete system for the hydrogen production. A technical overview of the technology was carried out, explaining all the working principles of the electrochemical device. Hence, a mathematical model was developed accounting for the deviations of the cell voltage, Faraday efficiency and hydrogen in oxygen content; these parameters were evaluated considering the effect of temperature, pressure and current density, except for the Faraday efficiency, where no appreciable change due to pressure could be detected. The formula for the cell voltage accounts also for the variations of electrolyte concentration and distance of the electrodes. A Matlab regression procedure is proposed for the reliable evaluation of the model parameters; experimental data evaluated at different temperatures and pressures is used. A Matlab model is implemented in order to estimate the operational parameters, changing the input conditions. The model is of particular relevance in the estimation of the hydrogen production and the stack temperature increase. The subroutine Aspen Custom Modeler is used in order to design the electrolyzer stack block for Aspen Plus. A complete system model is implemented in Aspen Plus, accounting for separation and drying units for hydrogen and oxygen. This model is able to predict more accurately the operational parameters of the stack and the hydrogen outlet flow, at the end of the separation and drying steps.

The parametric study conducted revealed that the temperature increase results in a lower stack voltage. A reduction was also noticed in the stack power, greater for higher current densities. Besides, temperature showed to reduce the production of excess heat, increasing the electricity converted into energy useful for the process. The Faraday efficiency is helped by temperature just at low current density, and the H₂O increases with temperature. As a consequence the hydrogen flow rate is reduced. The pressure does not affect the Faraday efficiency. Stack voltage, stack power and gas impurities increase with increasing pressure, leading to a

lower hydrogen flow rate. Results show that the positive effect of temperature is stronger than the negative effect of pressure. In the investigated ranges, an increase of temperature and pressure will lead to a decrease in the energy consumption. In particular, the best point of operation for the considered alkaline electrolysis system is revealed to be at $T = 80 \text{ }^\circ\text{C}$, $p = 5 \text{ bar}$, and a current density of about $i = 0.2 \text{ A/m}^2$, reaching a global efficiency of 67.5% and a specific consumption of 4.4 kWh/Nm^3 . The model developed could be considered reliable and accurate, inside the range limits. The comparison of the model with experimental data shows a close correlation.

5.1 Future developments

Aim of future researches could be the generalization of the mathematical model. The oxygen diffusion in the cathode could be modeled. The benefits are a better prediction of the outlet cathode stream composition and the limiting of the gas mixtures inside the safety limits. The same model for HTO could be extended to OTH calibrating the new model on experimental data. A further future topic could be the creation of a commercial-like drying and purification system. It could be used for the prediction of the outlet hydrogen purity. The principal advantage could be that of using the model for predicting hydrogen production for those end uses where the H_2 purity is imperative, like for fuel cell applications. Alkaline electrolyzers could have problems related to ramping and power quality. The present model is able to predict only steady state operations; a transient model would be crucial for determining the AEL behaviour with fluctuating power source, as RES.

Appendix A

Consideration of similar technologies

A.1 Comparison with different electrolysis solutions

Water electrolysis is mainly grouped in three categories of devices: alkaline electrolyzers, proton exchange electrolyzers, and high temperature electrolyzers. The main distinction depends on the temperature employed in the process and in the electrolyte technology, which influences the charge carrier species.

AELs is the most mature technology concerning electrolyzers. Nowadays they represent also the most effective solution. A longer life could be experienced, leading to a lower lifetime cost. Advance alkaline electrolyzers are also the most suitable for large scale application (*MW*) [16]. The need for liquid water as electrolyte is the main reason for the temperature limitations. The purity of hydrogen and oxygen is elevated; however the water fed has to be significantly pure, with an electric conductivity below $5 \mu S/cm$ [16].

PEM electrolyzers use a polymer electrolyte for the ion conduction. The most used membrane is Nafion, as for PEM fuel cells [16]. Only deionized water is fed to the cell, at the anodic side, without any electrolytic addition; this is done to avoid the electrodes corrosion. The polymer membrane works as electrolyte and gas separator, reducing the complexity of the cell. The main requirements of a PEM electrolyzer are: having a good stability from the mechanical, thermal, chemical and oxidative point of view. It needs to have a good permeability to ions, but a low permeability to gases and electrons. A high stability to work at severe condition over time concludes the required specifications [49]. Advantages of PEM over AEL electrolyzers are the high purity of hydrogen gas produced, low gas crossover,

control over fluctuating power feeding, easy cleaning and maintenance, lower power consumption. Another characteristic is the high safety levels guaranteed by the low gas permeability, avoiding the creation of flammable mixture and making the operation possible at very low current densities [16]. Main drawbacks are limited lifetime, high investment costs and restricted production capacity, which makes this technology not so diffuse at the present moment.

Higher temperatures allow a reach of higher efficiencies. This is the concept behind the SOEC technology. Solid oxide electrolysis is a new concept and much of the relevant information come from the solid oxide fuel cells operated in a reverse mode [16]. Water, in form of high temperature steam, is fed to the cathode side, differently to other technologies. The solid oxide electrolyte is typically a thin layer of yttria-stabilized zirconia (*YSZ*). Steam electrolysis is able to reduce the energy requirements. From the thermodynamic point of view, the open circuit voltage diminishes with increasing temperature, while the thermoneutral voltage has the opposite effect. The result is a shift of the energy need; a great part of it could be supplied in the form of heat at high temperatures. This feature makes SOEC particularly attractive when coupled with a high temperature heat source; such as geothermal, nuclear and concentrated solar power [16]. Other than the less energy requirements compared to low temperature electrolysis, SOEC has the advantage of being able to reach a higher efficiency (59% at 1000°C [49]). The main issues concern the thermal stability and sealing, which make the lifetime of SOEC lower compared to low temperature electrolyzer. Additionally the hydrogen produced must be subjected to processing stages to remove the steam. Consequently the costs for high temperature electrolysis are not competitive nowadays with the main opponents.

The table below (A.1) resumes the principal characteristic for the three different electrolysis technologies. Despite the complete water splitting reaction being the same in each of the processes, the half reactions at the anode and cathode differ consistently, because the charge carrier changes. The temperature is another discriminating factor which distinguishes the low-medium temperature electrolysis to the high temperature process.

A.2 Comparison within different alkaline electrolyzers

Differences could be noted between different alkaline electrolyzers. A first distinction could be made on the base of the architecture; the electrolysis cell configuration could be monopolar or bipolar. The main advantage of the first configuration is in the easiness of fabrication and maintenance. A disadvantage consists of the high electrical currents reached at low voltages, which can cause large ohmic losses [11].

Table A.1: Comparison between different types of water electrolysis. Basic chemical reaction and operating temperature range [49].

| Electrolysis technology | Alkaline Electrolysis | Membrane Electrolysis | High Temperature Electrolysis |
|--|--|---|--|
| Anode Reaction Oxygen Evolution Reaction (OER) | $2OH^- \rightarrow \frac{1}{2}O_2 + H_2O + 2e^-$ | $H_2O \rightarrow \frac{1}{2}O_2 + 2H^+ + 2e^-$ | $O^{2-} \rightarrow \frac{1}{2}O_2 + 2e^-$ |
| Cathode Reaction Hydrogen Evolution Reaction (HER) | $2H_2O + 2e^- \rightarrow H_2 + 2OH^-$ | $2H^+ + 2e^- \rightarrow H_2$ | $H_2O + 2e^- \rightarrow H_2 + O^{2-}$ |
| Charge Carrier | OH^- | H^+ | O^{2-} |
| Operating Temperature Range | $40 \div 90^\circ C$ | $20 \div 100^\circ C$ | $700 \div 1000^\circ C$ |

Bipolar electrolysis cells are preferred nowadays, because they permit the reduction of the ohmic losses. On the other side they demand much greater precision in design and manufacturing to prevent the electrolyte and gas leakage between cells [33].

Another distinction could be made based on the operating conditions. In particular:

- operating cell voltage: maintaining operating cell voltage as low as possible is needed in order to increase the efficiency of the electrolyzer.
- operating current density: increasing the operating current imply an increase in the rate of the hydrogen production; a higher current density corresponds to a greater electrochemical reactions rate. However, it increases the bubble formation. A compromise is needed between gas production rates and energy efficiency.
- operating stack temperature: a higher temperature of the stack decreases the equilibrium voltage. However, it increases the water evaporation rate and challenges the structural integrity of materials employed, in particular the diaphragm.
- operating pressure: pressurizing the electrolysis cell acts reducing the bubbles' size, minimizing ohmic losses. However, pressure does not have a significant effect on the final efficiency [78]. Higher pressure demands for more durable diaphragm.
- type and concentration of electrolyte: good conductance helps ionic transfer,

also influencing the electrical resistance of the electrolyte [31]. It is essential to work in the maximum conduction region of the solution.

- electrodes stability: the electrodes need to be designed in order to be resistant in alkali corrosive environments [32].
- water quality: magnesium and calcium could block on surface of electrode or diaphragm. Chloride ions are oxidised when exceeding a limiting current density, leading to formation of corrosive components [32].

Bibliography

- [1] Emanuele Taibi, Raul Miranda, Wouter Vanhoudt, Thomas Winkel, Jean-Christophe Lanoix, and Frederic Barth. «Hydrogen from renewable power: Technology outlook for the energy transition». In: (2018) (cit. on pp. 1–3).
- [2] Fuel Cell and Hydrogen Joint Undertaking. «Hydrogen Roadmap Europe: A Sustainable Pathway for the European Energy Transition». In: (2019) (cit. on pp. 1, 2).
- [3] IEA. *The Future of Hydrogen*. 2019. URL: <https://www.iea.org/reports/the-future-of-hydrogen> (cit. on p. 2).
- [4] Mustafa Balat. «Potential importance of hydrogen as a future solution to environmental and transportation problems». In: *International journal of hydrogen energy* 33.15 (2008), pp. 4013–4029 (cit. on p. 2).
- [5] Petros A Pilavachi, Anatoli I Chatzipanagi, and Antonia I Spyropoulou. «Evaluation of hydrogen production methods using the analytic hierarchy process». In: *International Journal of hydrogen energy* 34.13 (2009), pp. 5294–5303 (cit. on p. 2).
- [6] BA Kimball and SB Idso. «Increasing atmospheric CO₂: effects on crop yield, water use and climate». In: *Agricultural water management* 7.1-3 (1983), pp. 55–72 (cit. on p. 2).
- [7] Jamie D Holladay, Jianli Hu, David L King, and Yong Wang. «An overview of hydrogen production technologies». In: *Catalysis today* 139.4 (2009), pp. 244–260 (cit. on pp. 3, 4).
- [8] Marc Marsidi. *Technology factsheet - POLYMER ELECTROLYTE MEMBRANE (PEM) HYDROGEN INSTALLATION - SMALL-SCALE*. 2019. URL: <https://energy.nl/wp-content/uploads/2019/01/Polymer-electrolyte-membrane-PEM-hydrogen-installation-%E2%80%93-small-scale.pdf> (cit. on p. 6).

-
- [9] Binod Koirala. *Technology factsheet - SOLID-OXIDE ELECTROLYSIS*. 2020. URL: <https://energy.nl/wp-content/uploads/2019/01/Polymer-electrolyte-membrane-PEM-hydrogen-installation-%5C%E2%5C%80%5C%93-small-scale.pdf> (cit. on p. 6).
- [10] Agata Godula-Jopek. *Hydrogen production: by electrolysis*. John Wiley & Sons, 2015 (cit. on p. 6).
- [11] Øystein Ulleberg. «Modeling of advanced alkaline electrolyzers: a system simulation approach». In: *International journal of hydrogen energy* 28.1 (2003), pp. 21–33 (cit. on pp. 7, 14, 31, 34, 35, 37, 38, 40, 65).
- [12] Merit Bodner, Astrid Hofer, and Viktor Hacker. «H₂ generation from alkaline electrolyzer». In: *Wiley Interdisciplinary Reviews: Energy and Environment* 4.4 (2015), pp. 365–381 (cit. on pp. 7, 8).
- [13] Sergio Trasatti. «Work function, electronegativity, and electrochemical behaviour of metals: III. Electrolytic hydrogen evolution in acid solutions». In: *Journal of Electroanalytical Chemistry and Interfacial Electrochemistry* 39.1 (1972), pp. 163–184 (cit. on p. 8).
- [14] Marc TM Koper. «Thermodynamic theory of multi-electron transfer reactions: Implications for electrocatalysis». In: *Journal of Electroanalytical Chemistry* 660.2 (2011), pp. 254–260 (cit. on p. 8).
- [15] J Kubisztal and A Budniok. «Study of the oxygen evolution reaction on nickel-based composite coatings in alkaline media». In: *International journal of hydrogen energy* 33.17 (2008), pp. 4488–4494 (cit. on p. 9).
- [16] Alfredo Ursua, Luis M Gandia, and Pablo Sanchis. «Hydrogen production from water electrolysis: current status and future trends». In: *Proceedings of the IEEE* 100.2 (2011), pp. 410–426 (cit. on pp. 10, 12, 15, 17, 18, 21, 26, 64, 65).
- [17] Ernesto Amores, Jesus Rodriguez, and Christian Carreras. «Influence of operation parameters in the modeling of alkaline water electrolyzers for hydrogen production». In: *International Journal of Hydrogen Energy* 39.25 (2014), pp. 13063–13078 (cit. on pp. 12, 34, 37, 42).
- [18] Rodney L LeRoy, Christopher T Bowen, and Donald J LeRoy. «The thermodynamics of aqueous water electrolysis». In: *Journal of the Electrochemical Society* 127.9 (1980), p. 1954 (cit. on pp. 12, 15, 36).
- [19] RL LeRoy. «Industrial water electrolysis: present and future». In: *International Journal of Hydrogen Energy* 8.6 (1983), pp. 401–417 (cit. on pp. 12, 30, 31).

- [20] Mitja Mori, Tilen Mržljak, Boštjan Drobnič, and Mihael Sekavčnik. «Integral characteristics of hydrogen production in alkaline electrolyzers». In: *Strojniški vestnik-Journal of Mechanical Engineering* 59.10 (2013), pp. 585–594 (cit. on p. 14).
- [21] John H Perry. *Chemical engineers' handbook*. 1950 (cit. on p. 15).
- [22] A Ursua. «Hydrogen production with alkaline electrolyzes: Electrochemical modelling, electric power supplies and integration with renewable energies». In: *Ph. D. dissertation, Dept. Electr. Electron. Eng., Public Univ. Navarra, Pamplona, Spain* (2010) (cit. on pp. 16, 26).
- [23] Z Abdin, CJ Webb, and E MacA Gray. «Modelling and simulation of an alkaline electrolyser cell». In: *Energy* 138 (2017), pp. 316–331 (cit. on pp. 16, 18, 20, 34).
- [24] Kai Zeng and Dongke Zhang. «Recent progress in alkaline water electrolysis for hydrogen production and applications». In: *Progress in energy and combustion science* 36.3 (2010), pp. 307–326 (cit. on p. 17).
- [25] Amitava Roy, Simon Watson, and David Infield. «Comparison of electrical energy efficiency of atmospheric and high-pressure electrolyzers». In: *International Journal of Hydrogen Energy* 31.14 (2006), pp. 1964–1979 (cit. on p. 18).
- [26] Allen J Bard, Larry R Faulkner, et al. «Fundamentals and applications». In: *Electrochemical methods* 2.482 (2001), pp. 580–632 (cit. on p. 19).
- [27] Dang Saebea, Chakkrapong Chaiburi, and Suthida Authayanun. «Model based evaluation of alkaline anion exchange membrane fuel cells with water management». In: *Chemical Engineering Journal* 374 (2019), pp. 721–729 (cit. on p. 19).
- [28] Shih-Chieh Tu, Varadarajan Ravindran, and Massoud Pirbazari. «A pore diffusion transport model for forecasting the performance of membrane processes». In: *Journal of Membrane Science* 265.1-2 (2005), pp. 29–50 (cit. on p. 19).
- [29] Maximilian Schalenbach, Geert Tjarks, Marcelo Carmo, Wiebke Lueke, Martin Mueller, and Detlef Stolten. «Acidic or alkaline? Towards a new perspective on the efficiency of water electrolysis». In: *Journal of The Electrochemical Society* 163.11 (2016), F3197 (cit. on p. 19).
- [30] JW Veldsink, Rudolf MJ Van Damme, GF Versteeg, Willibrordus Petrus Maria Van Swaaij, et al. «The use of the dusty-gas model for the description of mass transport with chemical reaction in porous media». In: *Chemical Engineering Journal-Including Biochemical Engineering Journal* 57.2 (1995), pp. 115–126 (cit. on p. 19).

-
- [31] Mingyong Wang, Zhi Wang, Xuzhong Gong, and Zhancheng Guo. «The intensification technologies to water electrolysis for hydrogen production—A review». In: *Renewable and Sustainable Energy Reviews* 29 (2014), pp. 573–588 (cit. on pp. 21, 24–28, 67).
- [32] Kai Zeng and Dongke Zhang. «Recent progress in alkaline water electrolysis for hydrogen production and applications». In: *Progress in energy and combustion science* 36.3 (2010), pp. 307–326 (cit. on pp. 22, 23, 27, 32, 67).
- [33] WH Smyrl, JOM Bockris, BE Conway, E Yeager, and RE White. «Comprehensive Treatise of Electrochemistry». In: *Plenum Press, New York* 4 (1981), p. 116 (cit. on pp. 22, 66).
- [34] SK Mazloomi and Nasri Sulaiman. «Influencing factors of water electrolysis electrical efficiency». In: *Renewable and Sustainable Energy Reviews* 16.6 (2012), pp. 4257–4263 (cit. on pp. 24, 25).
- [35] N Nagai, M Takeuchi, T Kimura, and T Oka. «Existence of optimum space between electrodes on hydrogen production by water electrolysis». In: *International journal of hydrogen energy* 28.1 (2003), pp. 35–41 (cit. on p. 24).
- [36] J Udagawa, P Aguiar, and NP Brandon. «Hydrogen production through steam electrolysis: Model-based steady state performance of a cathode-supported intermediate temperature solid oxide electrolysis cell». In: *Journal of Power Sources* 166.1 (2007), pp. 127–136 (cit. on p. 24).
- [37] Kazuo Onda, Takahiro Kyakuno, Kikuo Hattori, and Kohei Ito. «Prediction of production power for high-pressure hydrogen by high-pressure water electrolysis». In: *Journal of power sources* 132.1-2 (2004), pp. 64–70 (cit. on p. 24).
- [38] N Nagai, M Takeuchi, T Kimura, and T Oka. «Existence of optimum space between electrodes on hydrogen production by water electrolysis». In: *International journal of hydrogen energy* 28.1 (2003), pp. 35–41 (cit. on pp. 25, 37).
- [39] National Center for Biotechnology Information. *PubChem Water (compound)*. 2021. URL: <https://pubchem.ncbi.nlm.nih.gov/compound/Water> (cit. on p. 27).
- [40] National Center for Biotechnology Information. *PubChem Hydrogen (compound)*. 2021. URL: <https://pubchem.ncbi.nlm.nih.gov/compound/783> (cit. on p. 27).
- [41] Daisuke Kiuchi, Hisayoshi Matsushima, Yasuhiro Fukunaka, and Kazuhiko Kuribayashi. «Ohmic resistance measurement of bubble froth layer in water electrolysis under microgravity». In: *Journal of The Electrochemical Society* 153.8 (2006), E138 (cit. on p. 27).

- [42] Roberto F De Souza, Janine C Padilha, Reinaldo S Gonçalves, and Jairton Dupont. «Room temperature dialkylimidazolium ionic liquid-based fuel cells». In: *Electrochemistry Communications* 5.8 (2003), pp. 728–731 (cit. on p. 28).
- [43] C Lagrost, D Carrie, M Vaultier, and Ph Hapiot. «Reactivities of some electrogenerated organic cation radicals in room-temperature ionic liquids: toward an alternative to volatile organic solvents?» In: *The Journal of Physical Chemistry A* 107.5 (2003), pp. 745–752 (cit. on p. 28).
- [44] Philipp Haug, Matthias Koj, and Thomas Turek. «Influence of process conditions on gas purity in alkaline water electrolysis». In: *International Journal of Hydrogen Energy* 42.15 (2017), pp. 9406–9418 (cit. on pp. 29, 34, 42).
- [45] Volkmar Schröder, Bernd Emonts, Holger Janßen, and H-P Schulze. «Explosion limits of hydrogen/oxygen mixtures at initial pressures up to 200 bar». In: *Chemical Engineering & Technology: Industrial Chemistry-Plant Equipment-Process Engineering-Biotechnology* 27.8 (2004), pp. 847–851 (cit. on pp. 29, 53).
- [46] Maximilian Schalenbach, Marcelo Carmo, David L Fritz, Jürgen Mergel, and Detlef Stolten. «Pressurized PEM water electrolysis: Efficiency and gas crossover». In: *International Journal of Hydrogen Energy* 38.35 (2013), pp. 14921–14933 (cit. on p. 29).
- [47] Marcelo Carmo, David L Fritz, Jürgen Mergel, and Detlef Stolten. «A comprehensive review on PEM water electrolysis». In: *International journal of hydrogen energy* 38.12 (2013), pp. 4901–4934 (cit. on p. 29).
- [48] Sergey A Grigoriev, Pierre Millet, SV Korobtsev, VI Porembskiy, M Pepic, C Etievant, C Puyenchet, and VN Fateev. «Hydrogen safety aspects related to high-pressure polymer electrolyte membrane water electrolysis». In: *International Journal of Hydrogen Energy* 34.14 (2009), pp. 5986–5991 (cit. on p. 29).
- [49] MD Rashid, Mohammed K Al Mesfer, Hamid Naseem, and Mohd Danish. «Hydrogen production by water electrolysis: a review of alkaline water electrolysis, PEM water electrolysis and high temperature water electrolysis». In: *International Journal of Engineering and Advanced Technology* (2015) (cit. on pp. 29–31, 64–66).
- [50] Akiyoshi Manabe, M Kashiwase, T Hashimoto, T Hayashida, A Kato, Kazuhiro Hirao, Ikuo Shimomura, and Ikuo Nagashima. «Basic study of alkaline water electrolysis». In: *Electrochimica Acta* 100 (2013), pp. 249–256 (cit. on pp. 30, 31).
- [51] VM Rosa, MBF Santos, and EP Da Silva. «New materials for water electrolysis diaphragms». In: *International Journal of Hydrogen Energy* 20.9 (1995), pp. 697–700 (cit. on p. 30).

- [52] J Kerres, G Eigenberger, S Reichle, V Schramm, K Hetzel, W Schnurnberger, and I Seybold. «Advanced alkaline electrolysis with porous polymeric diaphragms». In: *Desalination* 104.1-2 (1996), pp. 47–57 (cit. on p. 30).
- [53] Stefania Marini, Paolo Salvi, Paolo Nelli, Rachele Pesenti, Marco Villa, Mario Berrettoni, Giovanni Zangari, and Yohannes Kiros. «Advanced alkaline water electrolysis». In: *Electrochimica Acta* 82 (2012), pp. 384–391 (cit. on p. 31).
- [54] Monica Sanchez, Ernesto Amores, David Abad, Carmen Clemente-Jul, and Lourdes Rodriguez. «Development and Experimental Validation of a Model to Simulate an Alkaline Electrolysis System for Production of Hydrogen Powered by Renewable Energy Sources». In: Springer. 2019, pp. 358–368 (cit. on pp. 32, 34, 36, 42, 58–61).
- [55] Xiaohong Li, Frank C Walsh, and Derek Pletcher. «Nickel based electrocatalysts for oxygen evolution in high current density, alkaline water electrolyzers». In: *Physical Chemistry Chemical Physics* 13.3 (2011), pp. 1162–1167 (cit. on p. 32).
- [56] Derek Pletcher and Xiaohong Li. «Prospects for alkaline zero gap water electrolyzers for hydrogen production». In: *International Journal of Hydrogen Energy* 36.23 (2011), pp. 15089–15104 (cit. on p. 32).
- [57] Li Xiao, Shuai Zhang, Jing Pan, Cuixia Yang, Minglong He, Lin Zhuang, and Juntao Lu. «First implementation of alkaline polymer electrolyte water electrolysis working only with pure water». In: *Energy & Environmental Science* 5.7 (2012), pp. 7869–7871 (cit. on p. 32).
- [58] M Hammoudi, C Henao, K Agbossou, Y Dube, and ML Doumbia. «New multi-physics approach for modelling and design of alkaline electrolyzers». In: *International Journal of Hydrogen Energy* 37.19 (2012), pp. 13895–13913 (cit. on pp. 33, 36).
- [59] Amitava Roy, Simon Watson, and David Infield. «Comparison of electrical energy efficiency of atmospheric and high-pressure electrolyzers». In: *International Journal of Hydrogen Energy* 31.14 (2006), pp. 1964–1979 (cit. on p. 33).
- [60] Jaroslaw Milewski, Giulio Guandalini, and Stefano Campanari. «Modeling an alkaline electrolysis cell through reduced-order and loss-estimate approaches». In: *Journal of Power Sources* 269 (2014), pp. 203–211 (cit. on p. 33).
- [61] Martin David, Hernan Alvarez, Carlos Ocampo-Martinez, and Ricardo Sanchez-Pena. «Phenomenological based Model of Hydrogen production using an Alkaline self-pressurized Electrolyzer». In: *2019 18th European Control Conference (ECC)*. IEEE. 2019, pp. 4344–4349 (cit. on p. 33).

- [62] Martin David, Hernan Alvarez, Carlos Ocampo-Martinez, and Ricardo Sanchez-Pena. «Dynamic modelling of alkaline self-pressurized electrolyzers: a phenomenological-based semiphysical approach». In: *International Journal of Hydrogen Energy* 45.43 (2020), pp. 22394–22407 (cit. on p. 33).
- [63] Alfredo Ursua and Pablo Sanchis. «Static–dynamic modelling of the electrical behaviour of a commercial advanced alkaline water electrolyser». In: *International journal of hydrogen energy* 37.24 (2012), pp. 18598–18614 (cit. on p. 34).
- [64] Monica Sanchez, Ernesto Amores, David Abad, Lourdes Rodriguez, and Carmen Clemente-Jul. «Aspen Plus model of an alkaline electrolysis system for hydrogen production». In: *International Journal of Hydrogen Energy* 45.7 (2020), pp. 3916–3929 (cit. on pp. 34–36, 38, 39, 45).
- [65] Monica Sanchez, Ernesto Amores, Lourdes Rodriguez, and Carmen Clemente-Jul. «Semi-empirical model and experimental validation for the performance evaluation of a 15 kW alkaline water electrolyzer». In: *International Journal of Hydrogen Energy* 43.45 (2018), pp. 20332–20345 (cit. on pp. 34–38, 42, 51, 57).
- [66] PM Dieguez, A Ursua, P Sanchis, C Sopena, E Guelbenzu, and LM Gandia. «Thermal performance of a commercial alkaline water electrolyzer: experimental study and mathematical modeling». In: *international journal of hydrogen energy* 33.24 (2008), pp. 7338–7354 (cit. on pp. 34, 40, 41).
- [67] Xiaojun Shen, Xiaoyun Zhang, Tek Tjing Lie, and Guojie Li. «Mathematical modeling and simulation for external electrothermal characteristics of an alkaline water electrolyzer». In: *International Journal of Energy Research* 42.12 (2018), pp. 3899–3914 (cit. on pp. 34, 40).
- [68] W Hug, H Bussmann, and A Brinner. «Intermittent operation and operation modeling of an alkaline electrolyzer». In: *International journal of hydrogen energy* 18.12 (1993), pp. 973–977 (cit. on pp. 35, 42).
- [69] Roman Klyuev, Mariet Madaeva, and Marem Umarova. «Mathematical modeling of specific power consumption of electrolyzers». In: *2020 International Ural Conference on Electrical Power Engineering (UralCon)*. IEEE. 2020, pp. 356–361 (cit. on p. 35).
- [70] RJ Gilliam, JW Graydon, DW Kirk, and SJ Thorpe. «A review of specific conductivities of potassium hydroxide solutions for various concentrations and temperatures». In: *International Journal of Hydrogen Energy* 32.3 (2007), pp. 359–364 (cit. on p. 37).
- [71] W Hug, J Divisek, J Mergel, W Seeger, and H Steeb. «Highly efficient advanced alkaline electrolyzer for solar operation». In: *International journal of hydrogen energy* 17.9 (1992), pp. 699–705 (cit. on pp. 38, 42).

- [72] Dohyung Jang, Hyun-Seok Cho, and Sanggyu Kang. «Numerical modeling and analysis of the effect of pressure on the performance of an alkaline water electrolysis system». In: *Applied Energy* 287 (2021), p. 116554 (cit. on p. 39).
- [73] Frank P Incropera, David P DeWitt, Theodore L Bergman, Adrienne S Lavine, et al. *Fundamentals of heat and mass transfer*. Vol. 6. Wiley New York, 1996 (cit. on p. 41).
- [74] H Janssen, JC Bringmann, B Emonts, and Volkmar Schröder. «Safety-related studies on hydrogen production in high-pressure electrolyzers». In: *International Journal of Hydrogen Energy* 29.7 (2004), pp. 759–770 (cit. on p. 42).
- [75] Chau-Chyun Chen and Yuhua Song. «Generalized electrolyte-NRTL model for mixed-solvent electrolyte systems». In: *AIChE Journal* 50.8 (2004), pp. 1928–1941 (cit. on p. 45).
- [76] Cummins. *Hystat alkaline electrolyzers - Specs sheet*. 2020. URL: <https://www.cummins.com/sites/default/files/2021-08/cummins-hystat-30-specsheet.pdf> (cit. on p. 57).
- [77] Nel Hydrogen. *The World's Most Efficient and Reliable Electrolysers - Specs sheet*. 2019. URL: <https://nelhydrogen.com/wp-content/uploads/2020/03/Electrolysers-Brochure-Rev-C.pdf> (cit. on p. 57).
- [78] Derek Pletcher and Frank C Walsh. *Industrial electrochemistry*. Springer Science & Business Media, 2012 (cit. on p. 66).